Dissolved benthic phosphate, iron and carbon fluxes in the Mauritanian upwelling system and implications for ongoing deoxygenation

U. Schroller-Lomnitz, C. Hensen, A.W. Dale, F. Scholz, D. Clemens, S. Sommer, A. Noffke, K. Wallmann

PII: S0967-0637(18)30039-6
DOI: https://doi.org/10.1016/j.dsr.2018.11.008
Reference: DSRI2981

To appear in: *Deep-Sea Research Part I*

Received date: 8 February 2018
Revised date: 13 August 2018
Accepted date: 19 November 2018

Cite this article as: U. Schroller-Lomnitz, C. Hensen, A.W. Dale, F. Scholz, D. Clemens, S. Sommer, A. Noffke and K. Wallmann, Dissolved benthic phosphate, iron and carbon fluxes in the Mauritanian upwelling system and implications for ongoing deoxygenation, *Deep-Sea Research Part I,* https://doi.org/10.1016/j.dsr.2018.11.008

Dissolved benthic phosphate, iron and carbon fluxes in the Mauritanian upwelling system and implications for ongoing deoxygenation

U. Schroller-Lomnitz[1], C. Hensen[1], A. W. Dale[1], F. Scholz[1], D. Clemens[1], S. Sommer[1], A. Noffke[2] and K. Wallmann[1]

[1]GEOMAR Helmholtz-Centre for Ocean Research Kiel, Wischhofstr. 1-3, 24148 Kiel

[2]Institut für Seenforschung (ISF) der LUBW, Argenweg 50/1, 88085 Langenargen, Germany

Correspondence to: Ulrike Lomnitz (ulomnitz@geomar.de)

Keywords: Benthic fluxes, Phosphate, Iron, Carbon, Mauritanian Upwelling, Oxygen Minimum Zone

1. Abstract

Benthic fluxes of total dissolved phosphate (TPO_4^{3-}), dissolved iron (Fe^{2+}), and dissolved inorganic carbon (DIC) were determined in situ using benthic chambers at nine stations along a depth transect between 47 and 1108 m water depth at 18°N off Mauritania (NW Africa) during the upwelling season in 2014 (RV Meteor cruise M107). Bottom water oxygen (O_2) concentrations were always ≥ 25 µM, and all fluxes (TPO_4^{3-}, Fe^{2+}, DIC) were consistently directed from the sediments into the bottom water. The highest benthic TPO_4^{3-} release of 0.2 ± 0.07 mmol m^2 d^{-1} was found at 47 m water depth (50 µM O_2). The highest diffusive Fe^{2+} flux of 0.03 mmol m^2 d^{-1}, determined from porewater Fe^{2+} concentrations, occurred at 67 m water depth (27 µM O_2). This was much lower than the detrital Fe supply as indicated by constant Fe/Al ratios along the depth transect. TPO_4^{3-} release rates decreased concurrently with DIC flux and water depth. A difference of up to one order of magnitude between benthic chamber and diffusive TPO_4^{3-} fluxes indicated that the total TPO_4^{3-} release was strongly enhanced by bioirrigation.

The observed fluxes were similar to those measured during an earlier cruise in 2011, generally indicating comparable release rates during both upwelling seasons. Furthermore, ex situ oxygen manipulation experiments showed an increase of the nutrient release (e.g. TPO_4^{3-}, Fe^{2+}) after seven days of anoxic bottom water conditions. The fluxes were enhanced by a factor of 1.4 for P and 7.3 for Fe compared to the measured release under natural conditions and reached values as high as those measured in the anoxic oxygen minimum zone off Peru. Our observations support the hypothesis that increasing deoxygenation of the oceans will likely enhance sedimentary TPO_4^{3-} and Fe^{2+} release and

thus contribute to a positive feedback mechanism with increasing nutrient levels and increased ocean productivity.

2. Introduction

Phosphorus (P) and iron (Fe) are limiting nutrients for oceanic primary production (Broecker, 1982; Martin, 1990). P mainly derives from chemical weathering of apatite on land and is discharged to the oceans by riverine transport (Ruttenberg, 2014). However, only about 10-30% of the total delivered P is reactive and potentially bioavailable. About 75% of this reactive P reaches the ocean, with the remaining 25% being scavenged and deposited in estuaries and coastal sedimentary environments (Paytan & McLaughlin, 2007).

Continental margins receive Fe mainly from weathered continental rocks by river discharge. In contrast, the open ocean is supplied by Fe oxyhydroxides from dust deposition, but only a small fraction (1-10%) of the Fe associated with dust is dissolvable and bioavailable (Jickells and Spokes, 2001). Therefore, Fe is the key limiting nutrient in about 30 to 40% of the world oceans (Boyd and Ellwood, 2010). Recently, it has been hypothesized that the benthic release of Fe^{2+} and other redox-sensitive nutrients in shelf areas represents a much larger source to the water column than dust deposition (Dale et al., 2015; Emerson, 2016). TPO_4^{3-} and Fe^{2+} release from marine sediments are strongly coupled because P is typically adsorbed to Fe (oxyhydr)oxides in oxic sediment and released to the pore water by the dissimilatory reductive dissolution of Fe (oxyhydr)oxides in anoxic sediments (Sundby et al., 1986; Slomp et al., 1998). Hence, both TPO_4^{3-} and Fe^{2+} release from marine sediments are enhanced in oceanic oxygen deficient areas such as the eastern boundary upwelling systems (EBUS) (Sundby et al., 1986; McManus et al., 1997; Severmann et al., 2010; Noffke et al., 2012) and may fuel surface water primary production in a positive feedback loop (Ingall and Jahnke, 1997; Wallmann, 2010; Scholz et al., 2014; Dale et al., 2015). Although, EBUS cover only 1% of the world's oceans, they contribute about 10-15 % to the total marine primary production and are economically important areas for commercial fisheries (Carr, 2002; Behrenfeld and Falkowski, 1997; Cropper et al., 2014 and references therein). Recent studies on ocean deoxygenation found a significant oxygen loss in the past decades and predict a further decline for the future (Stramma et al., 2008; Schmidtko et al., 2017). Hence, it is crucial to understand the mechanisms driving nutrient release from sediments and how this process may affect surface ocean primary production.

A crucial step into this direction is the measurement of natural benthic nutrient fluxes in oxygen-depleted upwelling areas. Here, we present a new comprehensive data set on TPO_4^{3-} and Fe^{2+} benthic release rates for the Mauritanian upwelling along a depth transect at 18°N ranging from 47 to 1108 m water depth (Fig. 1A, Tab. 1). The coastal region off Mauritania is part of an eastern boundary upwelling system that extends from 10°N to about 43°N. Seasonal upwelling of cold nutrient-rich waters favors high surface primary production rates of up to 1.7 g C m^{-2} d^{-1} (Carr, 2002), while south of 20° N there is a pronounced seasonal cycle (Barton et al., 1998). Favorable winds prevail primarily

from December to April. Poor ventilation and intense degradation of the organic detritus leads to strong oxygen consumption and minimum oxygen concentrations of about 30 µM below the surface mixed layer.

The goal of the present study was to identify the P and Fe sources as well as the processes controlling the magnitude of the fluxes. Furthermore, the data set is accompanied by TPO_4^{3-} and Fe^{2+} flux measurements conducted during a previous cruise to the same study area, enabling us to compare magnitudes and temporal variability. In addition, we conducted ex situ oxygen manipulation experiments on incubated sediment cores in order to estimate the potential for enhanced nutrient release under scenarios of further decreasing oxygen levels. These are conditions presently met at the Peruvian OMZ and we discuss reasons for different flux-magnitudes in both areas.

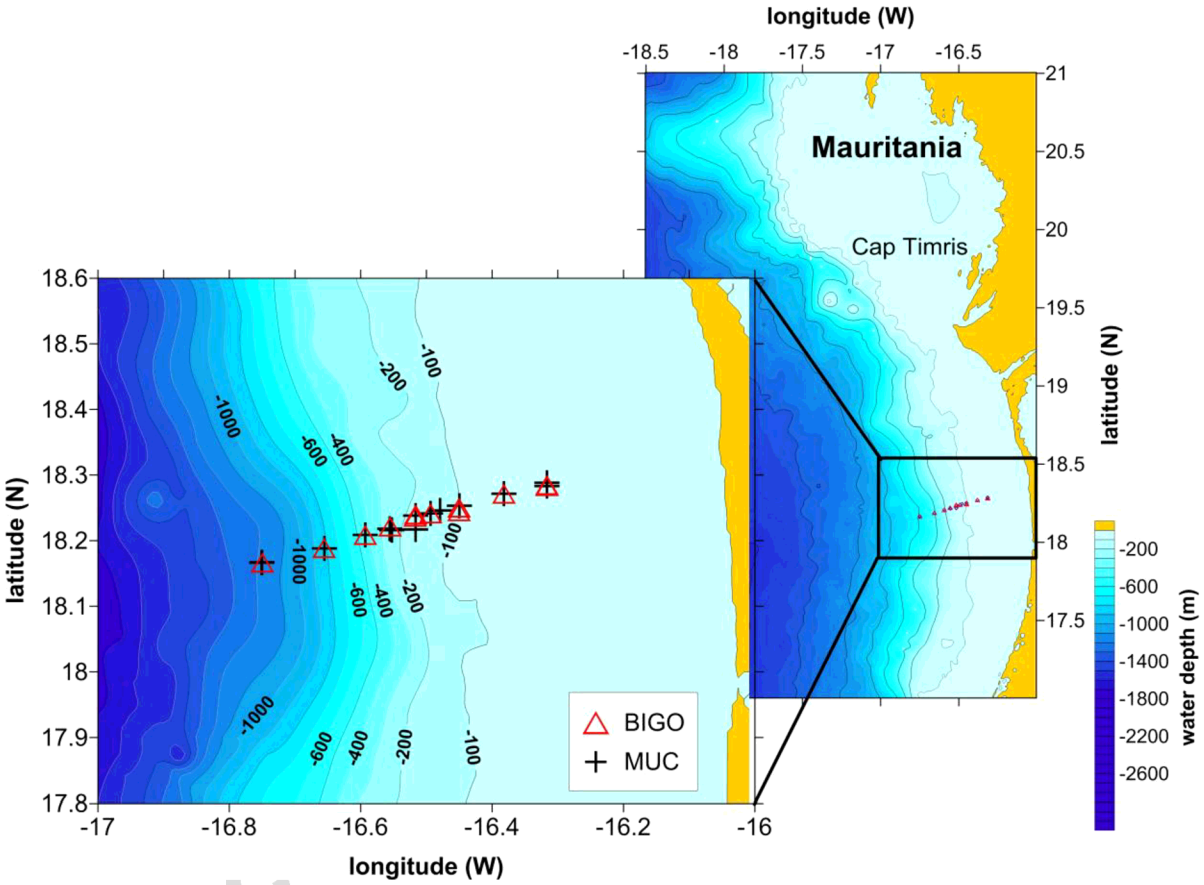

Figure 1: (A) Study area off Mauritania showing the 18°N depth transect and the deployed devices at each station during the M107 cruise (see Methods).

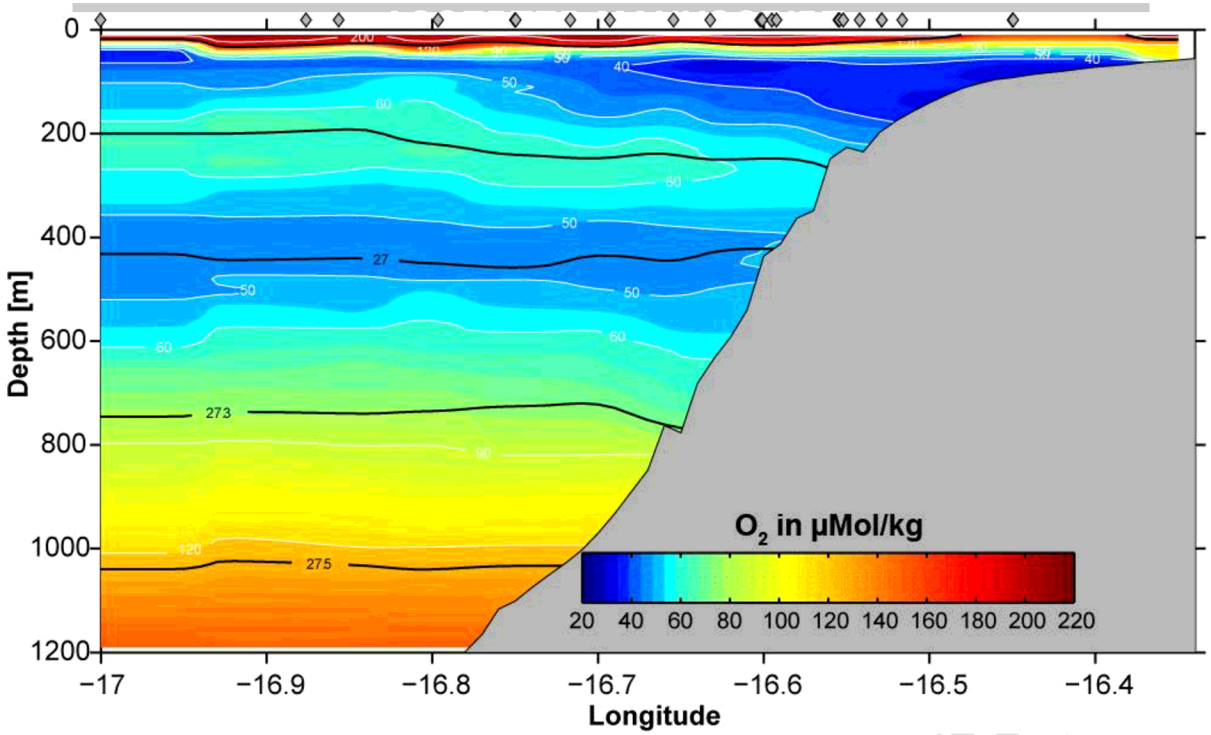

(**B**) Cross section across the 18°N depth transect showing O_2 concentrations (µmol kg^{-1}) from 8-14 June 2015 and the station locations across 18°N.

3. Study Area

The Mauritanian margin at 18°N lies within the Canary Upwelling System (11-35°N). Strong oxygen consumption takes place in the study area as a result of seasonal upwelling occurring from boreal winter to spring, leading to high primary production rates (1.7 g C m^{-2} d^{-1}, Carr, 2002 and 0.3 to 2.3 g C m^{-2} d^{-1}; Morel et al., 1996). The seasonality of the upwelling is driven by the migration of the Inter Tropical Convergence Zone (ITCZ) (Mittelstaedt, 1983). The upwelled South Atlantic Central Water (SACW) has a low salinity, is low in oxygen, and enriched in inorganic nutrients (Stramma et al., 2009). Trade winds export large quantities of Saharan dust into the waters off Mauritania, which is reflected by high solid phase Fe concentrations in the sediments (Mittelstaedt, 1983; Baker et al., 2006; Ohnemus & Lam, 2015).

The Mauritanian upwelling system is characterized by a moderate oxygen minimum zone (OMZ) between ~50 and 500 m water depth (Oschlies et al., 2008; Schmidtko et al., 2017). The lowest bottom water oxygen concentrations of ~30 µM occur between 200 and 600 m water depth (Fig. 1B, Tab. 1). Time series data over the last 50 years suggest that the oxygen concentration in the wider Western Tropical North Atlantic is apparently decreasing at a rate of 0.5 µmol kg^{-1} yr^{-1} (Stramma et al., 2008). Due to high biological productivity, the future of the regional fishery may be under threat by the ongoing deoxygenation (Pauly and Christensen, 1995).

The sediments in the study area are characterized by variable lithology. At water depths <100 m, sand accounts for up to 70 dry wt. % of the total particulate material. Between 170 and 255 m water depth, the sand and mud fractions are nearly equal. The sand fraction recovers at ~ 425 m water depth to 66

wt. % whereas mud dominates the sediments in deeper waters (~ 780 – 1120 m) where the sand content decreases to ~ 7 wt. % (Dale et al., 2014 and references therein). Sokoll et al. (2016) characterized sediments down to ~ 480 m water depth as permeable with a strong advective transport component in the porewater and at the sediment-water interface. Geochemically, the sediments are carbonate-rich and contain considerable amounts of biogenic silica and quartz (Hartmann et al., 1976). The particulate organic carbon content (POC) ranges between 1 and 3 % dry weight (Dale et al., 2014). The seafloor is densely covered by traces of burrow-dwelling macrofauna indicating that bioirrigation is likely an important process of solute exchange (Dale et al., 2014; Kirstensen et al., 2012). Tracer incubation experiments showed that bioirrigation by bivalves and polychaetes is most intense on the shelf and occurs down to ca. 15 – 20 cm depth (Gier et al., 2017).

4. Methods

The stations were chosen to coincide with a previous R/V Maria S. Merian cruise (MSM17-4), which was conducted during upwelling season in March/April 2011. To augment the database in shallow waters, three additional stations were sampled during the more recent R/V Meteor (M107) cruise during late to post upwelling season in May/June 2014. At each station sediments were sampled with a multiple-corer (MUC) and fluxes were measured using two GEOMAR BIGO (Biogeochemical Observatory) landers. Additionally, water column particles were sampled at two stations (47 and 236 m water depth) using a CTD/Rosette equipped with Niskin bottles. The ex situ sediment core incubation experiments were made on sediment cores sampled at 236 m water depth.

4.1. Porewater and solid phase analysis

Sediment cores were retrieved using a video-guided multiple-corer (MUC). After retrieval, all cores were immediately transferred to a cool room (12°C, mean bottom water temperature across the depth transect) and processed within 1-2 hours. The porewater was extracted using rhizons (type CCS from Rhizosphere with a pore size of 0.15 µm) for the sandy shelf and upper slope sediments (water depth < 400 m) (St. 1 – 6). The core liners were pre-drilled and the holes were masked with tape for placing of the rhizons after core recovery. The first 0.5 ml of porewater extruded was discarded. Porewater extraction using this method required up to 30 minutes, yielding about 10 ml of porewater at each depth interval. For muddier sediments below 400 m (St. 7 – 9), the cores were sectioned in an argon filled glove bag at a depth resolution of 0.5 or 1 cm at the surface to 2 cm at depth. The porewater was separated by centrifugation at 4000 rpm for 20 min, and then filtered through 0.2 µm cellulose-acetate filters under argon. Additional sediment sub-samples were taken at each sediment depth interval and stored refrigerated in pre-weighed, air-tight plastic cups for the determination of water content, porosity, total organic carbon (TOC) and solid phase constituents in the onshore laboratory (GEOMAR).

After extraction, porewater samples were immediately analyzed photometrically for dissolved TPO_4^{3-}, Fe^{2+}, NO_3^-, NO_2^-, and NH_4^+ (see further details in section 4.5). The analyses were performed according

to the standard techniques described in Grasshoff et al. (1999) and can be derived elsewhere (e.g. Scholz et al., 2011, Dale et al., 2014). Porewater samples were stored at 4 °.

The TOC content of freeze-dried and ground sediment samples was determined by flash combustion in a Carlo Erba Elemental Analyzer (NA 1500) with an analytical precision and detection limit of 0.04 wt. %. Samples were decalcified with 2.5 N HCl prior to analysis.

Total sediment digestions for elemental analysis of Fe and Al were conducted on one core from each water depth. About 100 mg of freeze-dried and ground sediment were digested in hydrofluoric acid (40 %, supra pure), nitric acid (65 %, sub-boiled distilled), and perchloric acid (60 %, supra pure). For quality control, the sediment reference standard SDO-1 (Devonian Ohio Shale) for organic rich sediments and the marine sediment reference standard MESS-3 were included in the analysis as well as methodological blanks. The Fe and Al content in the digestion solutions were measured using an inductively coupled plasma optical emission spectrometer (ICP-OES, Varian 720 ES). The relative standard deviation (RSD) for [Al] and [Fe] was < 1 %.

4.2. In situ TPO_4^{3-} and DIC flux measurements

In situ TPO_4^{3-} fluxes were determined using samples obtained from two landers, BIGO I and II at nine stations along a depth transect at 18°20' N at water depths of 47, 67, 91, 130, 171, 236, 412, 787 and 1096 m (Tab. 3). Each BIGO was equipped with two circular incubation chambers with an internal diameter of 28.8 cm and a total area of 651.4 cm^2 (Sommer et al., 2009). A TV-guided launching system allowed smooth emplacement of the observatories on the sea floor. During an initial time period of four hours, when the chambers were still not fully inserted into the sediment, the water inside the flux chamber was periodically replaced with ambient bottom water to remove particles that may have been suspended during the deployment on the sea floor. After the chamber was fully driven into the sediment, the chamber water was again replaced with ambient bottom water from outside the chamber to flush out solutes that might have been released from the sediment during chamber insertion. Over the incubation period of 48 hours, 8 sequential water samples were removed with glass syringes (volume ~ 47 ml). To monitor the ambient bottom water, eight additional glass syringe samples were taken. The TPO_4^{3-} standard series covered a concentration range from 0.05 to 3.5 µM. The fluxes were calculated from the slope of the linear regression of all eight data points vs. the sampling time and corrected for the water volume in the chamber and the dead volume (pre-filled with distilled water) of the 1m long Vygon tubes connecting the syringes with the flux chambers. The error caused by the dilution from the dead volume of distilled water in these tubes was corrected using the chloride concentration measured in the syringe samples and the ambient seawater. The resulting correction factor was multiplied with the solute concentration to adjust for the dilution by the distilled water from the Vygon tubes. For most sites, the reported benthic chamber fluxes were based on two replicate chamber measurements (i.e. two chambers per BIGO). The uncertainty reported for the TPO_4^{3-} fluxes is the difference between the minimum and maximum TPO_4^{3-} fluxes determined in the two benthic chambers.

Dissolved inorganic carbon (DIC) measurements were performed using a quadrupole membrane inlet mass spectrometer (MIMS, GAM200, In Process Instruments) as described by Sommer et al. (2017). The instrument was equipped with inline sample acidification to shift the carbonate system entirely to the volatile CO_2 species, which then was measured on the MIMS at a mass to charge ratio of 44 (Bell et al., 2011).

4.3. Diffusive Fe^{2+} flux calculation

No significant temporal change in Fe^{2+} concentrations could be detected in the benthic chambers, possibly as a result of dissolved Fe^{2+} adsorption to the walls of the glass syringes. Instead, the diffusive benthic Fe flux was calculated from pore water profiles by Fick's 1st law of diffusion:

$$(1)\quad Fe^{2+}\text{flux} = -\phi D_{Sed}\frac{d[C]}{dx}.$$

where ϕ is the porosity of the surface sediment and D_{Sed} is the diffusion coefficient of Fe^{2+} at the sediment-water interface. The term d[C]/dx denotes the concentration difference between the bottom water and the uppermost porewater sample divided by the depth below the seafloor (1 cm at St. 2, 3, 4 and 6, 0.5 cm elsewhere). The molecular diffusion coefficient D_{SW} was taken from Boudreau (1997) and corrected for the in situ temperature (from CTD measurements) at each station and for salinity and pressure using the Stokes Einstein relationship (Li and Gregory, 1974). The resulting diffusion coefficients were corrected for sediment porosity (Boudreau, 1997):

$$(2)\quad D_{Sed} = \frac{D_{SW}}{1-\ln(\phi^2)}$$

Diffusive P fluxes were determined in the same way as a comparison with the benthic chamber fluxes.

4.4. Water column particle sampling and analysis

Suspended and sinking particles were sampled by filtration (0.7 µm Whatman GF/F) of 4 to 12 L of water that was retrieved from Niskin bottles attached to a CTD/Rosette at 47 and 236 m water depth. The particles were analyzed in duplicate for total particulate phosphorus (TPP), particulate inorganic phosphorus (PIP) and particulate organic carbon (POC) using standard combustion and colorimetric methods (Aspila, 1976) as described in detail by Lomnitz et al. (2016). Measurements were calibrated against eight standards ranging from 5 to 100 µM PO_4^{3-}, prepared from a Merck phosphate stock solution.

POC was determined as described above.

4.5. Ex situ O_2 manipulation experiments

We conducted an ex situ on board experiment to test the effect of anoxia on TPO_4^{3-} and Fe^{2+} release from the sediments at 237 m water depth in undisturbed sediment cores and without visual signs for bioirrigating organisms. Prior to the deployment, the MUC liners were prepared with calibrated oxygen sensitive spots (Presens Sensor type PSt3, detection limit 15 ppb, accuracy ± 0.4% O_2 at 20.9

% O_2 and 0.05% O_2 at 0.2% O_2) for non-invasive O_2 measurements during the entire experiment. Three replicate sediment cores (A, B, and C) were transferred to the cold room (12°C, i.e. in situ temperature) and allowed to stand (while stirred) for 24h before the experiment was started.

Core A and B were kept oxic for approximately 20 h before the oxygen concentration was lowered by carefully bubbling argon gas through the overlying bottom water. The anoxic phase of core A and B was maintained for at least 9.5 days. Core B was then oxygenated again and kept under oxic conditions for approximately 3 days. Core C was a control core maintained at an oxygen concentration similar to the in situ bottom water concentration. The enclosed waterbody was ventilated with air or argon to regulate the oxygen concentrations. During the experimental period (14.5 d), water samples were taken at regular intervals. After each sampling, the water volume equivalent to the sample volume of ~ 20 ml was refilled with bottom water from reservoir bags. NO_3^- levels in the control core were maintained between 10 and 20 µM by addition of $NaNO_3$ stock solution (16.13 mM).

Measurements of NO_3^-, NO_2^-, NH_4^+ and PO_4^{3-} in the water samples were performed on board once a day using a QuAAtro autoanalyzer (Seal Analytical) with a precision of ±0.1 µmol l^{-1}, ±0.1 µmol l^{-1}, ±0.2 µmol l^{-1} and ±0.24 µmol l^{-1}, respectively. For ferrous iron concentration analysis, subsamples of 0.5 to 1 ml were complexed with Ferrozin and determined photometrically (Stookey, 1970). Sample cups were flushed with Argon after filling to minimize oxidation artefacts. The detection limit of this method is about 0.1µM.

5. Results

5.1. Porewater distributions

Porewater TPO_4^{3-} showed similar trends as Fe^{2+} (Fig. 2). The concentration peaks coincided or were slightly shifted below the Fe^{2+} maxima. At water depths between 47 and 169 m, the concentrations varied around 10 to 15 µM and remained more or less constant to the bottom of the core. Below 169 m water depth, concentrations increased to 30 µM and the maxima were shifted down-core. Porewater H_2S concentrations measured in cores from 47 to 129 m water depth showed a notable increase below 10 cm. The highest concentration of ~ 90 µM occurred at St. 1 in ~ 15 cm sediment depth.

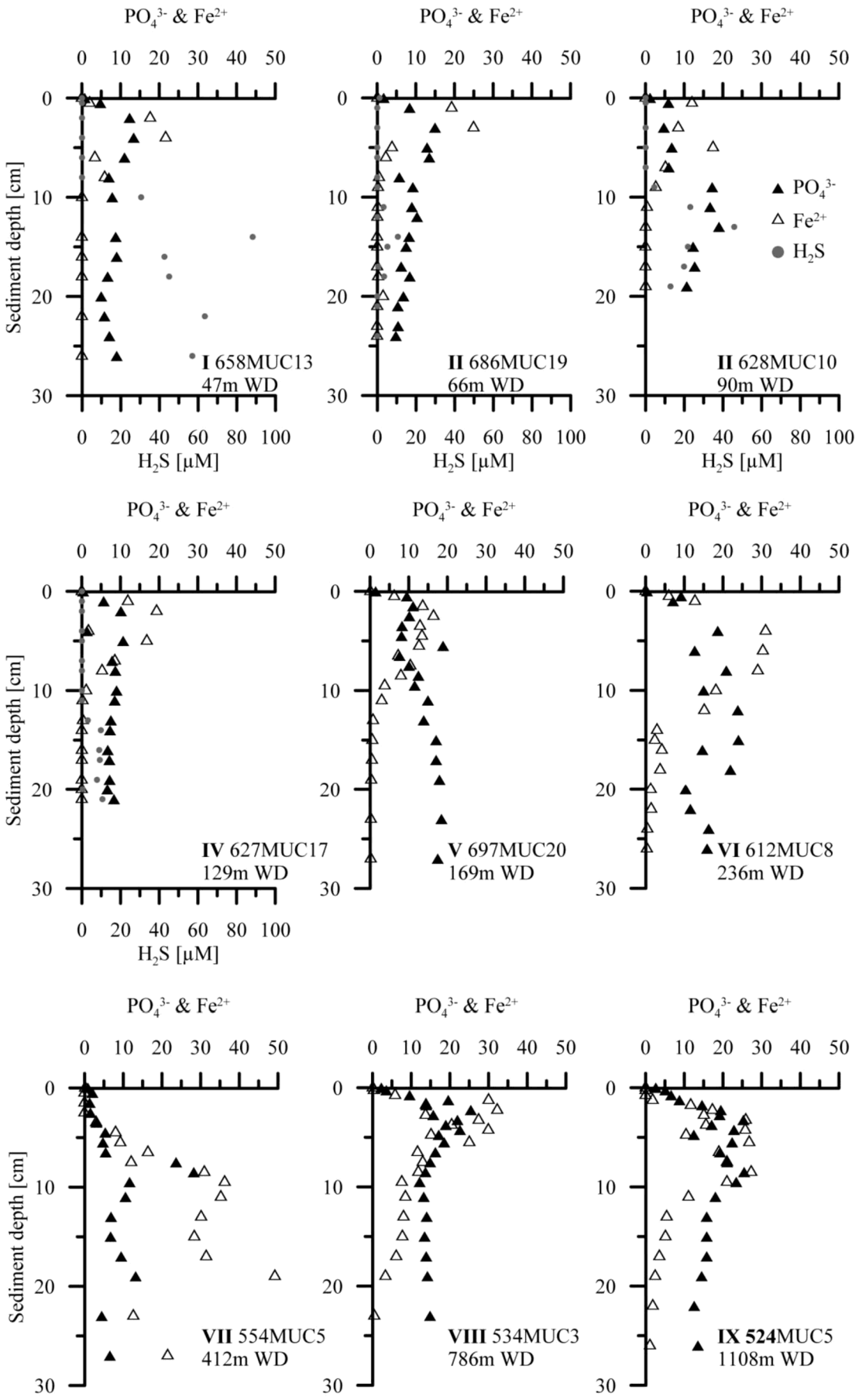

Figure 2: Porewater profiles of TPO_4^{3-} (closed triangles), Fe^{2+} (open triangles) and H_2S (solid grey circles) in µM for all stations along the 18°N depth transect. The first data point of each solute

indicates the bottom water concentration obtained from the overlying water in the multiple-corers. H_2S was only measured at station 1 to 4. Each graph contains information on the core's station number and the water depth (WD) it was retrieved from in the bottom right corner.

5.2. Solid phase distributions

The average solid phase Fe, P and Al sediment content increased with water depth along the transect (Fig. 3, Supplement 1). The Fe and Al profiles showed no trend with increasing sediment depth. Solid phase P concentrations decreased in the top 5 cm of sediment at St. 4, 5, 8 and 9 and remained constant to the core end. At St. 7, both Al and P content increased from the surface sediment to ~ 10 cm depth and then decreased slightly. The average Fe/Al ratio for all analysed samples was 0.55 while the ratio was slightly higher at St. 3 to 6 and slightly lower at St. 1 (Fig. 2). All ratios were consistent with the broad range of lithogenic Fe/Al ratios in the study area (0.4 and 0.8; Scheuvens et al., 2013). Atmospheric dust originating in the Saharan desert has been identified as the main source of Fe to sediments on the Mauritanian continental margin (Scheuvens et al., 2013).

Similar to Fe/Al, sedimentary Ti/Al ratios were in the range of values published for the lithogenic background (0.04 – 0.08, Scheuvens et al., 2013) (Tab. 2, Fig. 4). The highest ratios (0.07 and 0.08) observed at shallow water depths between 47 and 236 m. At greater water depths (400 – 1100 m) the Ti/Al ratios decreased to ~ 0.06. A decrease in Ti/Al ratios means a change from coarser to finer grain sizes.

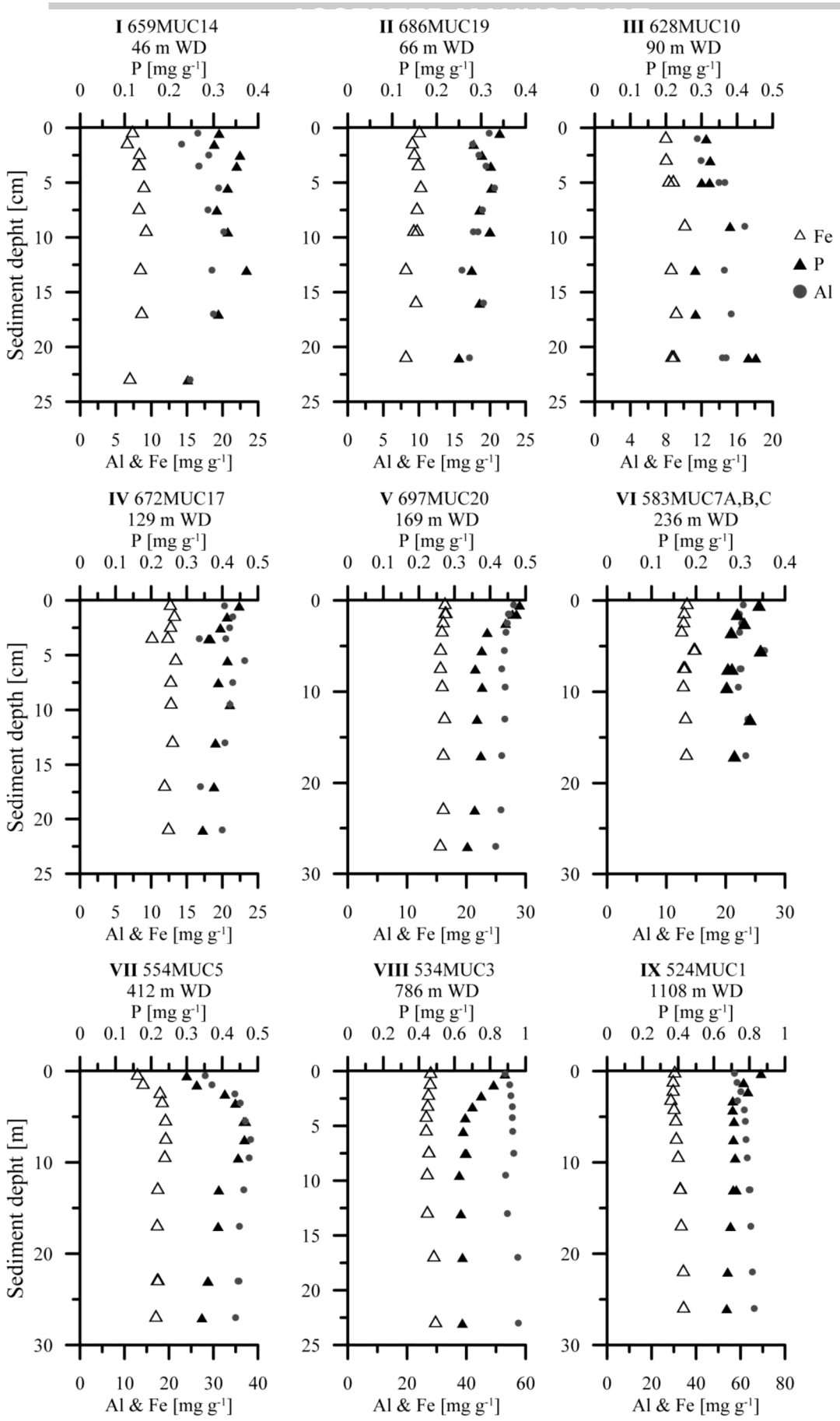

Figure 3: Solid phase P (µmol g^{-1}), Fe and Al (mmol g^{-1}) contents in sediments along the 18°N depth transect. Note the change in scales at the two deepest stations.

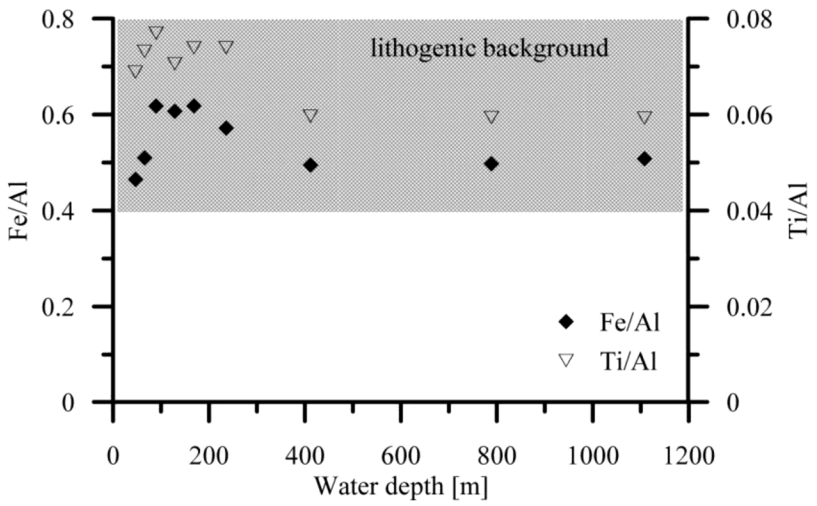

Figure 4: Mean Fe/Al and Ti/Al ratios versus water depth. The grey shaded area indicates the lithogenic background ratio for Fe/Al. Ti/Al serves as a qualitative proxy for grain size along the depth transect. Each graph contains information on the core's station number and the water depth (WD) it was retrieved from in the bottom right corner.

5.3. Sedimentary particulate organic carbon (POC) content

The POC content of the sediments increased with water depth (Supplement 1). Lowest values of 0.55 wt. % were measured at St. 2 and 3 (66 and 90 m water depth). POC concentrations range between 0.9 to 1.3 wt. % at the other stations. A sharp increase occurred at ~ 786 and 1108 m water depth where POC content increased to 2.6 and 3.3 wt. %, respectively.

Sedimentary POC/TPP ratios in the surface sediments (Tab. 4) were constantly below the empirically derived stoichiometric ratio (106:1) of carbon to phosphorus found in marine phytoplankton (Redfield, 1963). With the exception of station I, the ratios slightly increased with sediment depth as well as with increasing water depth. The mean POC/TPP ratio of all sediment samples was 76.

5.4. In situ benthic fluxes

The total benthic chamber TPO_4^{3-} fluxes off Mauritania were directed to the water column (positive values) at all stations (Fig. 5 A, Tab. 3, Supplement 2). The highest TPO_4^{3-} flux of 0.2 ± 0.07 mmol m^{-2} d^{-1} was determined at 47 m water depth (St. 1) where bottom water oxygen concentration was 50 µM. With the exception at 91 m water depth (St. 3), the TPO_4^{3-} release rates decreased gradually with increasing water depth to values of 0.05 ± 0.005 at the deepest stations. A comparatively low TPO_4^{3-} flux of 0.09 ± 0.045 mmol m^{-2} d^{-1} was measured at St. 3 (90 m water depth) coinciding with the lowest measured bottom water oxygen concentration (25µM) along the depth transect (Fig. 5 A).

DIC fluxes decreased strongly from about 20 to 10 mmol m^{-2} d^{-1} between 47 and 91 m (Fig. 5 B). Below that depth, DIC fluxes decreased more smoothly reaching values of about 5 mmol m^{-2} d^{-1} at 423 m and remained almost constant at larger water depths.

5.5. Diffusive benthic iron flux

The diffusive Fe^{2+} fluxes ranged between 0.03 to 0 mmol m^{-2} d^{-1} at 47 m (St. 1) and 1108 m (St. 9), respectively (Fig. 5B, Tab. 3). In analogy to the in situ benthic P flux, Fe release decreased to a local minimum at station 3 (91 m water depth). Below this water depth, the Fe^{2+} fluxes increased again down to 169 m, before decreasing slightly in deep waters. The 786 m site was an exception (St. 8), where the Fe release increased to a relatively high value of 0.05 mmol m^{-2} d^{-1}.

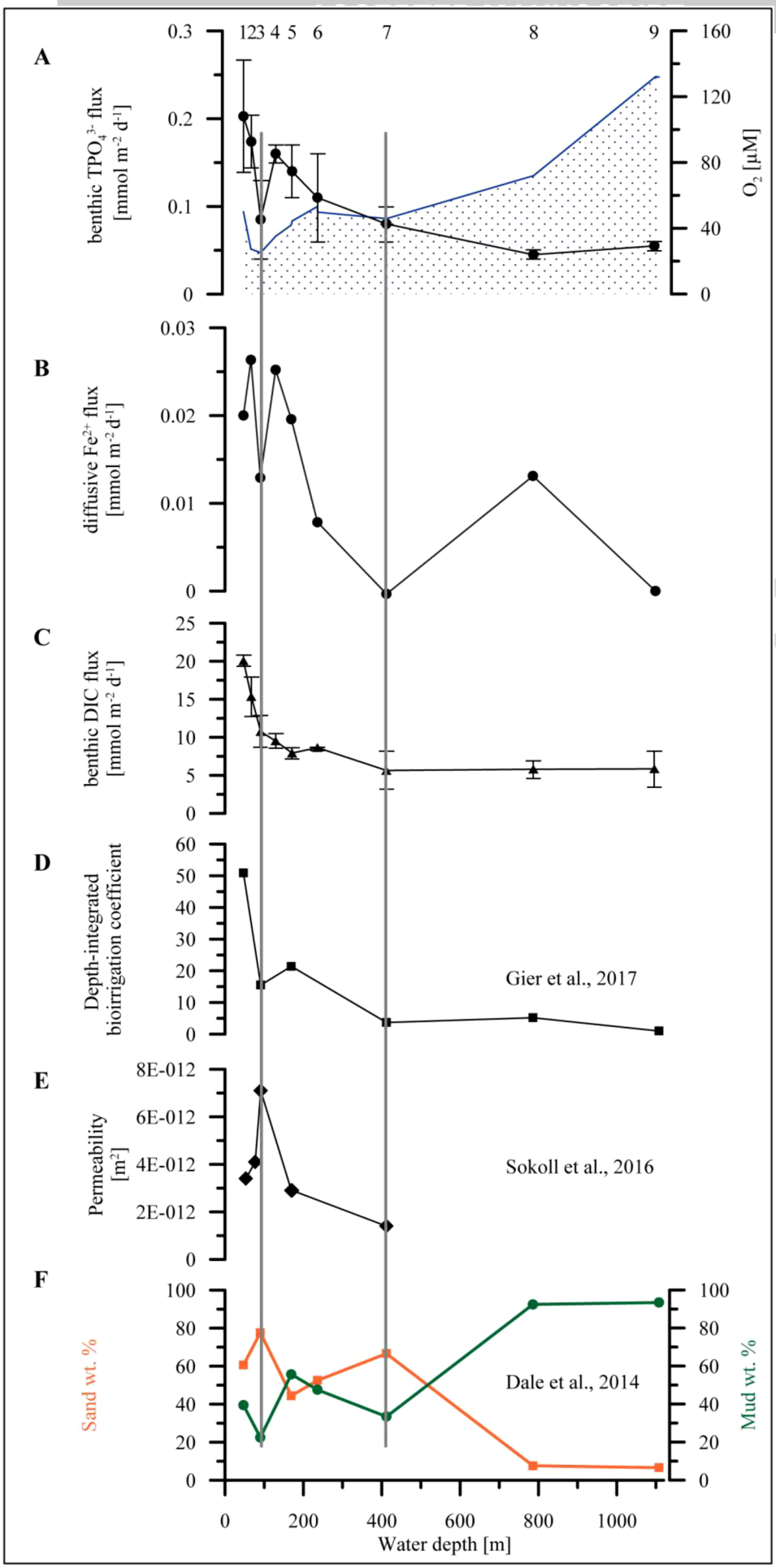
A
benthic TPO_4^{3-} flux [mmol m^{-2} d^{-1}]
O_2 [µM]
1 2 3 4 5 6 7 8 9
B
diffusive Fe^{2+} flux [mmol m^{-2} d^{-1}]
C
benthic DIC flux [mmol m^{-2} d^{-1}]
D
Depth-integrated bioirrigation coefficient
Gier et al., 2017
E
Permeability [m^2]
Sokoll et al., 2016
F
Sand wt. %
Mud wt. %
Dale et al., 2014
Water depth [m]

Figure 5: Overview of various parameters along the along the depth transect at 18°N: (A) Benthic chamber TPO_4^{3-} flux in mmol m^{-2} d^{-1} (line and circles) and bottom water oxygen concentration (O_2 µM, stippled blue area); (B) diffusive Fe^{2+} fluxes in mmol m^{-2} d^{-1}; (C) benthic DIC fluxes in mmol m^{-2} d^{-1}; (D) depth-integrated bioirrigation coefficient (dimensionless) normalized to the deepest station (Gier et al., 2017); (E) permeability in m^2 determined during cruise MSM17-4 at the same sites as visited during M107 (Sokoll et al., 2016); (F) sand (orange stripes)/mud (black stripes) distribution in wt.% described by Dale et al. (2014), derived from samples taken during MSM17-4 at the same stations as sampled during M107. Numbers on top denote the station numbers that are also given in Table 1. The grey lines at 90 and 412 m water depths depict bottom water oxygen minima observed during cruise M107 (see also Fig. 1B).

5.6. Water column particles

The measured concentrations of TPP, PIP, POP and POC in the sampled particulate matter are reported in Supplement 3. The TPP concentrations were much higher at St. 1(47 m water depth) compared to St. 6 (236 m water depth).

PIP concentrations were highest in the surface waters at St. 1 (0.3 µM) and lowest (0.014 µM) at 225 m water depth at St. 6. On average, PIP comprised 49 % of TPP. As POP is operationally defined as the difference between TPP and PIP. Hence, the opposite trends are valid for POP concentrations in the water column.

Very high POC concentrations of 51 and 27 µM were measured at 10 and 20 m water depth at St. 1. Lowest concentrations of ~ 4 µM were found at 150 m water depth at St. 6.

The mean POC/TPP, POC/PIP and POC/POP ratios were 134 ± 12, 310 ± 40 and 309 ± 87, respectively (Tab. 4).

5.7. Oxygen manipulation experiments

Results from the ex situ oxygen manipulation experiments on sediment cores from 237 m are shown in Figure 6. The initial Fe concentrations before oxygen started to decease were below detection limit in cores A, B and C. The initial TPO_4^{3-} concentrations were 1.6 µM in all three cores. These values were measured about 8 h after the first measurement allowing the system to settle following disturbances during core retrieval. The initial NO_3^- concentrations were > 20 µM. The drawdown of oxygen started after one day and lasted for another day until anoxic bottom water conditions were established. The accumulation of Fe^{2+} in the bottom waters started approximately 5 days later and that of TPO_4^{3-} 7.5 days later. The sharp increase in TPO_4^{3-} release began slightly after the point when NO_3^- was completely consumed and coincided with the beginning of a strong NH_4^+ release. NO_2^- concentrations were relatively constant throughout the experiment except for a consistent peak of 17 µM in core A and 13 µM in core B immediately after the point where NO_3^- became depleted. Dissolved Fe^{2+} was released from the sediments only after nitrate and nitrite were completely consumed.

Fe^{2+} and TPO_4^{3-} concentrations continued to increase at the time when core A incubation was ended, reaching 6.7 µM of Fe^{2+} and 8.9 µM of TPO_4^{3-}. NH_4^+ concentrations in this core increased to values of 77.7 µM.

Core B was re-oxygenated after ~ 10 days of anoxia by opening a small valve on the lid of the stirrer. (Note that the ephemeral O_2 peaks at 211 and 247 h are artefacts introduced during sub-sampling). The initial O_2 bottom water concentrations were reached after less than one day of oxygenation. TPO_4^{3-} concentrations then plateaued for ~ 1 day and started to slightly decrease thereafter but remained high at 3.3 µM after ~ 3 days of oxygenation. Fe^{2+} concentrations started to decrease after about half a day and ended at 0.7 µM when the experiment was stopped. Although Fe^{2+} concentrations were one order of magnitude larger than in the initial bottom water concentrations, the rate of Fe^{2+} depletion is faster than TPO_4^{3-}, indicating a stronger sensitivity to O_2. NO_3^- concentrations increased slightly coincidental with the addition of oxygen due to nitrification whereas the NH_4^+ release persisted until the end of the experiment.

In the oxygenated control core C, Fe and P concentrations stayed rather constant during the entire experiment duration at ~ 0.7 and ~ 1.1 µM, respectively. NO_3^- concentrations decreased monotonously due to ongoing denitrification and were increased artificially at ~80 hrs. NO_3^- then decreased in the second half of the experiment. NH_4^+ increased simultaneously to ~ 8.9 µM and remained at this value for the rest of the experiment. NO_2^- was not detected in the control core C during the entire incubation.

The diffusive Fe^{2+} and TPO_4^{3-} fluxes (Fig. 6, Tab. 5) were calculated from the slope of the increasing solute concentrations between the following time intervals: Fe^{2+} in core A from 133 to 247 h, in core B from 151 to 267 h; TPO_4^{3-} in core A from 97 to 255 h and in core B from 113 to 279 h. In the following, these fluxes are named 'potential' fluxes as they do not reflect measurements at naturally occurring environmental conditions during the cruise.

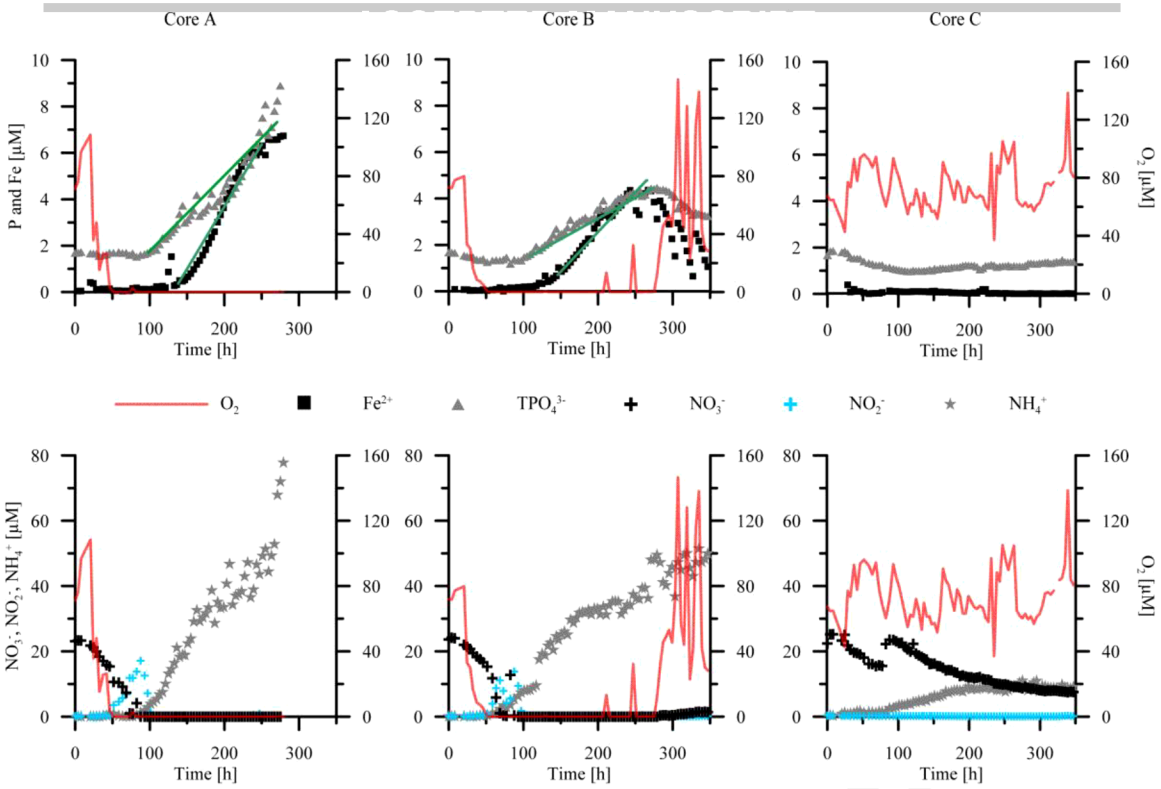

Figure 6: Bottom water concentrations of TPO_4^{3-}, Fe^{2+}, NO_3^-, NO_2^- and NH_4^+ (µM) during ex situ oxygen manipulation experiments in three multiple-cores (A, B and C). Core A was kept anoxic for the entire experiment duration whereas core B was oxygenated again after ~12.5 days. Core C was run as a control core with O_2 concentrations maintained at ca. 80 µM. The green lines in the upper two panels mark the slopes of the increasing solute concentrations in the above mentioned time intervals used for the calculation of the TPO_4^{3-} and Fe^{2+} release rates in core A and B (Tab. 5).

6. Discussion

6.1. TPO_4^{3-}, Fe^{2+}, and DIC release

Benthic TPO_4^{3-} release is mainly driven by organic matter remineralization in sediments and further enhanced by low oxygen concentrations in overlying bottom waters (Ingall and Jahnke, 1994). The magnitude of organic matter degradation can be estimated from the dissolved inorganic carbon (DIC) fluxes measured in situ. Both, DIC and TPO_4^{3-} fluxes decreased exponentially with water depth (Fig. 5A and C) indicating a strong coupling. If TPO_4^{3-} release would be driven by POC degradation alone, one would expect a relation of the DIC and the PO_4^{3-} fluxes according to Redfield (1963) with a C/P ratio of 106. However, the comparison of both fluxes shown in Figure 7 indicates higher TPO_4^{3-} release than expected from Redfield. Our in-situ flux data show that TPO_4^{3-} is preferentially released even though oxygen concentrations in ambient bottom water are higher than the threshold for enhanced TPO_4^{3-} release (20 µM) observed in previous studies (Wallmann, 2010).

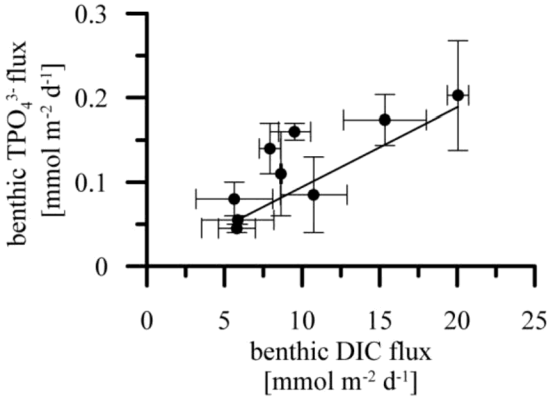

Figure 7: Benthic chamber TPO_4^{3-} vs. DIC fluxes (closed circles) and the theoretical TPO_4^{3-} fluxes that would derive from organic matter degradation according to Redfield composition (black line). The deviation from the measured and the theoretical fluxes indicates that further P sources than particulate organic phosphorus (POP) are needed to maintain the measured release rates.

The measured total benthic chamber TPO_4^{3-} fluxes exceed the diffusive fluxes by up to one order of magnitude, implying that the TPO_4^{3-} release is dominated by non-diffusive processes (Fig. 8, Tab. 3).

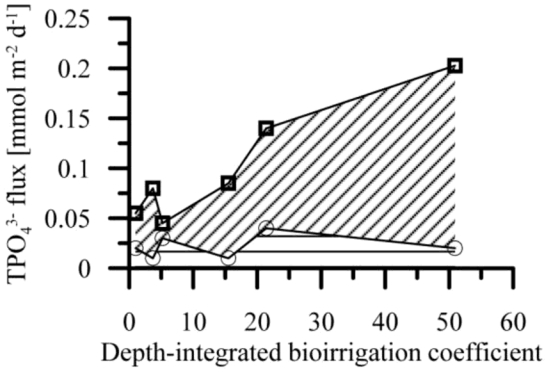

Figure 8: Benthic chamber (rectangles) and diffusive (circles) TPO_4^{3-} fluxes (mmol m^{-2} d^{-1}) plotted against the depth-integrated bioirrigation coefficient (dimensionless) normalized to the deepest station (Gier et al., 2017). Total benthic TPO_4^{3-} fluxes are significantly elevated at higher bioirrigation levels.

The high permeability of the sandy seafloor off Mauritania (Fig. 5 E, F) may allow bottom water to flow through surface sediments along horizontal pressure gradients induced by bottom currents and topography (Huettel et al., 2003, Sokoll et al., 2016). Moreover, sandy sediments are an indicator for strong bottom water currents, leading to fast POC degradation and erosive loss of the fine-grained material, which was observed for water depths down to 240 m along the depth transect (Dale et al., 2014, Sokoll et al., 2016). Measurements undertaken with an acoustic Doppler velocimeter revealed a high bottom water current velocity at 240 m water depth of up to 20 cm s^{-1} induced by internal waves (Sokoll et al., 2016). The bottom water current velocity ranged between 5 and 10 cm s^{-1}.However, high

sand content of the sediments on the Mauritanian shelf is also a result of episodically occurring events where high loads of sand are transported by winds from the adjacent Sahara desert to the ocean.

Apart from the high sand content, the seafloor of the Mauritanian shelf is densely populated by macrofauna and speckled by burrow holes (Dale et al., 2014). Along the depth transect, distinct traces of benthic organisms and their tracks were observed, possibly due to changes in sediment characteristics and bottom water oxygen concentrations. Many traces of organisms were found in the sediments with higher sand content, suggesting that these are responsible for enhanced bioirrigation in this area (Fig. 5D; Gier et al., 2017). Bioirrigating organisms, such as polychaetes and bivalves, exchange bottom and porewater by ventilating their burrows for feeding purposes and the impact of bioirrigation on solute exchange by burrowing animals is well recognized (e.g. Aller 1980; Dale et al., 2013, Norkko and Shumway, 2011, Meysman et al, 2006; Kristensen et al., 2012). The importance of bioirrigation (including physically induced water flow through permeable sediments; e.g. Huettel et al., 2003) in the working area is demonstrated in Figure 8, showing that total TPO_4^{3-} fluxes are significantly enhanced compared to diffusive fluxes when bioirrigation is high. Moreover, the lowest bottom water oxygen concentrations were found concurrent with a decrease of the bioirrigation coefficients and a sharp drop in TPO_4^{3-} release (Fig. 5 A and D). In contrast, the highest release rates offshore Peru are typically found at to the lowest bottom water oxygen concentrations (Lomnitz et al., 2016; section 6.2).

The offset from the Redfield ratio between in TPO_4^{3-} and DIC fluxes (Fig. 7) is reson to take a closer look at P sources and sedimentary P turnover. The inorganic P fraction (PIP) contributes significantly to the total P inventory of sediments off Mauritania. Our analyses revealed a mean PIP fraction of 75 % of the total sedimentary P inventory. The sedimentary PIP inventory can be enhanced by the conversion of POP into PIP while TPP remains constant; a process known as sink-switching (Ruttenberg and Berner, 1993; Faul et al., 2005). Most of the PIP formed in marine sediments is composed of carbonate fluoro-apatite (Ruttenberg and Berner, 1993). This authigenic mineral phase precipitates from ambient pore fluids that are enriched in dissolved phosphate due to POP degradation. Our water column particle and sediment composition data suggest that sink-switching occurs off Mauritania. We found that sediments were enriched in PIP and depleted in POP compared to water column particles (Tab. 4). Furthermore, our down-core data suggest that POP to PIP conversion takes place already at the sediment/water interface and intensifies with sediment depth (Tab. 4). A P mass balance was set up for the two stations in our study area where the water column was analyzed (47 and 236 m) considering the rain rate of TPP to the sediment, the benthic chamber release of dissolved TPO_4^{3-}, and TPP burial below the bioturbated zone (Tab. 6). At the shallow station where sediments do not accumulate because of strong bottom currents, the mass balance was closed within the error range of the benthic fluxes. This means that the rain rate of TPP to the seabed derived from the DIC flux and the TPP/POC ratio in water column particles was as high as the benthic chamber TPO_4^{3-} flux into the water column. At the deeper station where sediments accumulated at a high rate (0.35 cm yr^{-}

[1]), the mass balance was not closed because the TPP rain rate was smaller than the sum of the benthic TPO_4^{3-} release and TPP burial flux (Tab. 6). This observation may indicate that down-slope transport of TPP contributed significantly to the burial flux. The deficit may also be explained by a lower POC/TPP ratio in sinking particles reaching the seabed compared to the suspended particles that were sampled and analyzed in this study. Finally, it is possible that the high benthic fluxes measured during our cruise induce a decline in the TPP stock of surface sediments reflecting non-steady state conditions in P supply/release as postulated for the Peruvian OMZ (Lomnitz et al. 2016).

Benthic diffusive Fe^{2+} fluxes are mainly controlled by the availability of reactive Fe oxyhydroxides that are reductively dissolved during organic matter degradation (e.g. Froelich et al., 1979; Canfield et al., 1989). Bottom water oxygen concentrations below 20 µM also favor benthic Fe release (Dale et al., 2015). Although bottom waters off Mauritania are more oxic than this, we attempted to calculate the potential Fe^{2+} release across the sediment water interface from porewater profiles, being aware that this method cannot account for Fe precipitation at the very sediment surface preventing Fe^{2+} escape into bottom water.

Fe^{2+} release was induced by a shallow Fe reduction zone due to intense organic matter degradation in the surface sediments at St. 1 (47 m) to VI (236 m). However, the low Fe release at St. 3 is likely due to stronger oxygenated sediments caused by enhanced permeability and bioirrigation. Shale fragments of bivales were found in the entire sediment core. Hydrogen sulfide accumulation, produced by sulfate reduction, began at ~ 9 to 11 cm sediment depth (Fig. 2). In the transition zone between hydrogen sulfide and Fe-release above, precipitation of iron sulfides can be presumed. Below 250 m water depth, bottom water oxygen levels rose and organic carbon degradation decreased leading to a shift of the Fe reduction zone deeper into the sediments (~ 5 – 15 cm), and a decrease in Fe release (Fig. 2, 5 B & C). It is likely that a large fraction of the Fe^{2+} diffusing towards the sediment/water interface is oxidized and precipitated as ferric iron oxyhydroxide at the sediment surface before it can reach the overlying water column. However, a recent study of Klar et al. (2017) showed that dissolved Fe released from the sediments could be stabilized by complexation to organic ligands in oxic waters. Moreover, ferric iron nanoparticles may form during the oxidation process that may not settle instantaneously but may be transported over large distances before they are finally removed by particle scavenging (Raiswell and Canfield, 2012).

The flux peak calculated for St. 8 (786 m water depth) may result in a significant Fe release into the water column. Independent data of dissolved Fe in the water column revealed a dFe plume in the bottom waters of St. 8 coinciding with elevated $^{224}Ra/^{223}Ra$ ratios (Rapp, personal communication). Oceanic Ra originates from pore water release, sediment resuspension, and submarine groundwater discharge (Moore, 1987; Moore and Arnold, 1996b; Rama and Moore, 1996) and is therefore a suitable indicator for the origin of the Fe plume. Hence, in this case it is likely that a significant fraction of the diffusive iron flux is transported across the sediment/water interface into ambient

bottom waters probably as organic complex or nanoparticle. Nevertheless, this uncertainty clearly emphasizes the need for enhanced future efforts on the fate of iron released from marine sediments.

The mean Fe/Al ratio of all cores along the depth transect was 0.55, which is in the range of the reported background ratio of 0.4 to 0.8 (Fig. 4, Tab. 2). The large range of the Fe/Al background ratio is a result of the various rock and sediment types in the Sahara desert – the source area for the Fe supply. However, the sedimentary Fe/Al ratios are enriched in Fe compared to the average upper continental crust with a Fe/Al ratio of 0.44 (McLennan, 2001). Even higher average ratios of 0.61 were found at stations 3 to 5 although dissolved Fe was released from the sediments, indicating that detrital Fe supply is clearly exceeding the Fe release. Hence, the shifts in solid phase concentrations were likely an effect of increasing grain size induced by strong bottom water currents, since elevated Fe/Al ratios were found to be concurrent to enhanced Ti/Al ratios at St. 3 to V (Fig. 4; e.g. Boyle, 1983; Zabel et al., 1999).

TPO_4^{3-} and Fe^{2+} fluxes from early summer 2014 (M107), representing late to post upwelling conditions, were compared to fluxes measured during the upwelling season in spring 2011 (MSM17/4) at the same stations. Overall, the TPO_4^{3-} and Fe^{2+} fluxes from the two datasets are of the same order of magnitude (Fig. 9 and 10). However, the TPO_4^{3-} and Fe^{2+} release rates were consistently lower in water depths between 40 and 240 m during upwelling. This could be an effect of overall higher bottom water oxygen concentrations ($\geq$ 50 µM O_2) compared to the conditions during summer 2014 (Tab. 1) inhibiting benthic nutrient release to the overlying bottom waters. Only at 98 and 236 m water depth was the Fe^{2+} release during upwelling higher than in summer 2014. During M107, porewaters from cores at 66, 90 and 129 m water depth were sampled in 2 cm intervals by rhizones, whereas all other cores from M107 and MSM17-4 were sectioned in 1cm intervals. The diffusive Fe^{2+} fluxes determined during spring 2011 might thus be more realistic. Nevertheless, both datasets include the sharp decline of the Fe^{2+} flux at ~ 90 m water depth consolidating this feature and indicating long-term persistence. Furthermore, the unusually high Fe flux found at 789 m water depth was even higher in 2011. It remains unclear whether the decreased bottom water oxygen concentration in shallow waters and the slightly enhanced TPO_4^{3-} and Fe^{2+} release are a consequence of ongoing oxygen loss on the Mauritanian margin.

6.2. Comparison with the Peruvian Oxygen Minimum Zone

In this section, we compare comprehensive data sets of TPO_4^{3-} and Fe^{2+} fluxes of two prominent eastern boundary upwelling systems, the Mauritanian and Peruvian upwelling (Noffke et al, 2012; Lomnitz et al., 2016; Scholz et al, 2016). The most prominent difference between the two areas is the bottom water oxygen concentration. Mauritanian bottom waters O_2 concentrations did not fall below 20 µM (a threshold for the definition of an OMZ; Helly and Levin, 2004) at any time during our measuring campaigns. The lowest O_2 levels detected at ~ 90 m water depth were around 27 µM (M107 in 2014). In contrast, the Peruvian upwelling is highly dynamic where long-lasting periods of anoxic and nitrate-reducing (nitrogenous) conditions are interrupted by short-lived oxic and sulfidic events (Gutiérrez et al., 2008; Noffke et al., 2012; Schunk et al., 2013; Scholz et al., 2016; Sommer et al., 2016; Graco et al., 2017). Furthermore, the primary production rates on the Mauritanian margin are slightly lower (1.7 g C m^2 d^1 (Carr, 2002) and 0.3-2.3 g C m^{-2} d^{-1} (Morel et al., 1996)) than reported for Peru (1.8-3.6 g C m^2 d^1 (Dale et al., 2015 and references therein). However, given that TPO_4^{3-} and Fe^{2+} release rates are ultimately driven by POC degradation in the sediment, it is more meaningful to compare DIC fluxes rather than primary production rates. The DIC fluxes indicate a much higher organic matter rain rate and degradation rate at shallow water depths of about 70 m off Peru (65.9 ± 21 mmol $m^{-2}d^{-1}$; Dale et al., 2015) compared to Mauritania (15.3 ± 2.7 mmol $m^{-2}d^{-1}$). Furthermore, the benthic microbial community completely different. Dense mats of sulfide-oxidizing bacteria, which are ubiquitous on the Peruvian margin at water depths down to 300 m and likely have strong effect on

the P-cycle (Lomnitz et al., 2016), are absent off Mauritania, presumably due to relatively high bottom water O_2 concentrations.

Mauritanian and Peruvian TPO_4^{3-} release rates diverge mainly in water depth between 50 to 420 m (Fig. 9, Noffke et al., 2012; Lomnitz et al., 2016, this study). TPO_4^{3-} release measured off Peru is up to a factor of two higher than off Mauritania. Accordingly, the porewater TPO_4^{3-} concentrations reported off Peru were in general at least twice as high as off Mauretania (Noffke et al., 2012; this study).

As mentioned above, high POC degradation rates and low bottom water oxygen concentrations favor a strong TPO_4^{3-} release. However, also local features modulate the magnitude of the fluxes significantly. Off Peru, sulfide oxidizing bacteria have been suggested to play a key role in benthic P cycling (Lomnitz et al., 2016). Sulfur bacteria such as *Beggiatoa* or *Thiomargarita* are known to be adapted to the oscillating redox conditions, storing intracellular polyphosphates during oxic conditions and degrade these to gain energy when anoxic conditions occur (Schulz and Schulz, 2005; Brock and Schulz-Vogt, 2011). When polyphosphates are degraded, phosphate is released to the bottom water enhancing the benthic TPO_4^{3-} release. Such organisms are absent off Mauritania, but instead burrow dwelling macrofauna modulate TPO_4^{3-} release rates (see section 6.2.).

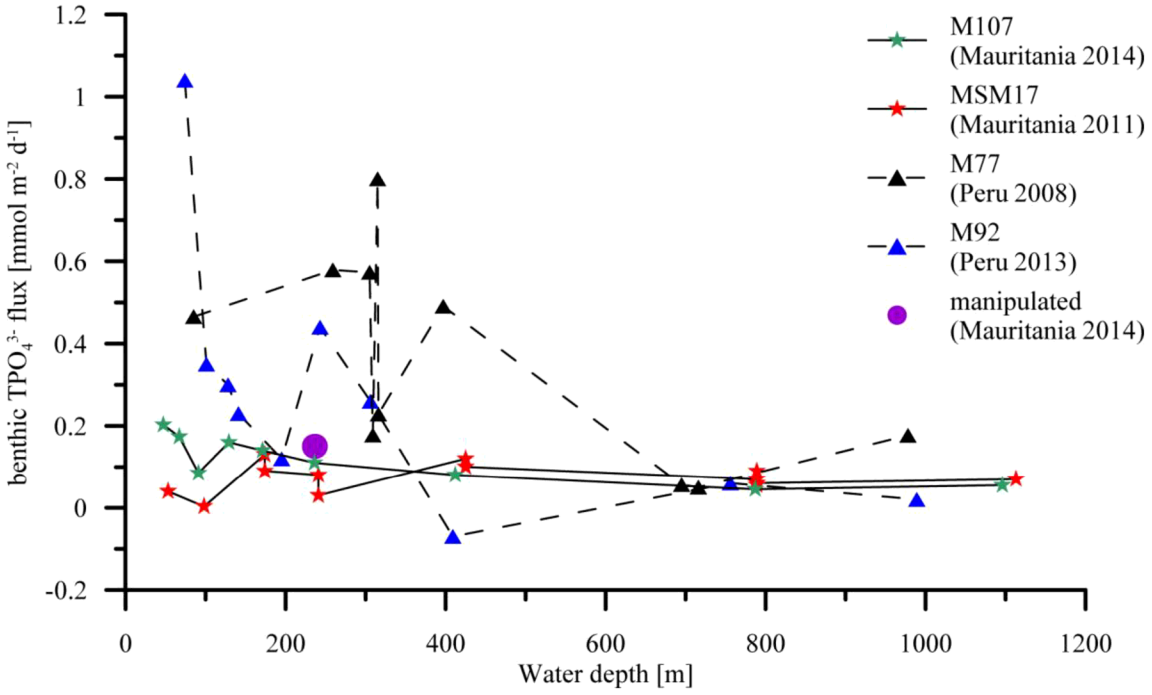

Figure 9: Benthic chamber TPO_4^{3-} fluxes (mmol m^{-2} d^{-1}) from Mauritania (MSM17/4 and M107) along the 18°N depth transect and from the Peruvian margin (M77 and M92) along 11 and 12°S depth transects. The single purple circle denotes the TPO_4^{3-} release determined from the O_2 manipulation experiments.

Despite considerable differences in the bottom water oxygen concentrations, the diffusive Fe^{2+} fluxes on the Mauritanian and Peruvian margins are in overall good agreement (Fig. 10). At first sight, the similarity of Fe^{2+} fluxes off Mauritania and Peru is remarkable. The porewater Fe^{2+} concentrations found off Mauritania were of the same magnitude or slightly lower as found in the porewaters off Peru (Noffke et al., 2012). However, during the M92 sampling campaign off Peru, weakly sulfidic waters and high porewater sulfide concentrations reduced diffusive Fe^{2+} fluxes on the shallow shelf (Scholz et al., 2016). In contrast, during the M77 Peru cruise (Noffke et al., 2012, 11° S, similar water depths) exceptionally high diffusive Fe^{2+} fluxes were observed at the shallow stations (~ 80 m water depth). As suggested by Noffke et al. (2012), this was due to an oxygenation event that took place shortly before the sampling campaign. During this event, dissolved Fe^{2+} was reoxidized and deposited at the seafloor thereby replenishing the highly reactive Fe inventory at the sediment surface. During the following anoxic period, the precipitated Fe oxyhydroxides were dissolved and released to the bottom water. Low Fe^{2+} fluxes in the Peruvian core OMZ measured during both cruises M77 and M92 were attributed to persistent anoxic bottom waters causing a depletion of the available Fe pool over time (Noffke et al., 2012; Scholz et al., 2011, 2014).

Overall, reduced Fe release during sulfidic bottom water conditions off Peru and slightly oxic bottom water conditions off Mauritania lead to comparable Fe^{2+} fluxes although major control parameters, such as the degradation rates of organic matter and the bottom water oxygen levels, were largely different. This observation highlights the complexity of predicting benthic Fe fluxes and the need for a better understanding of the interplay of major environmental control parameters.

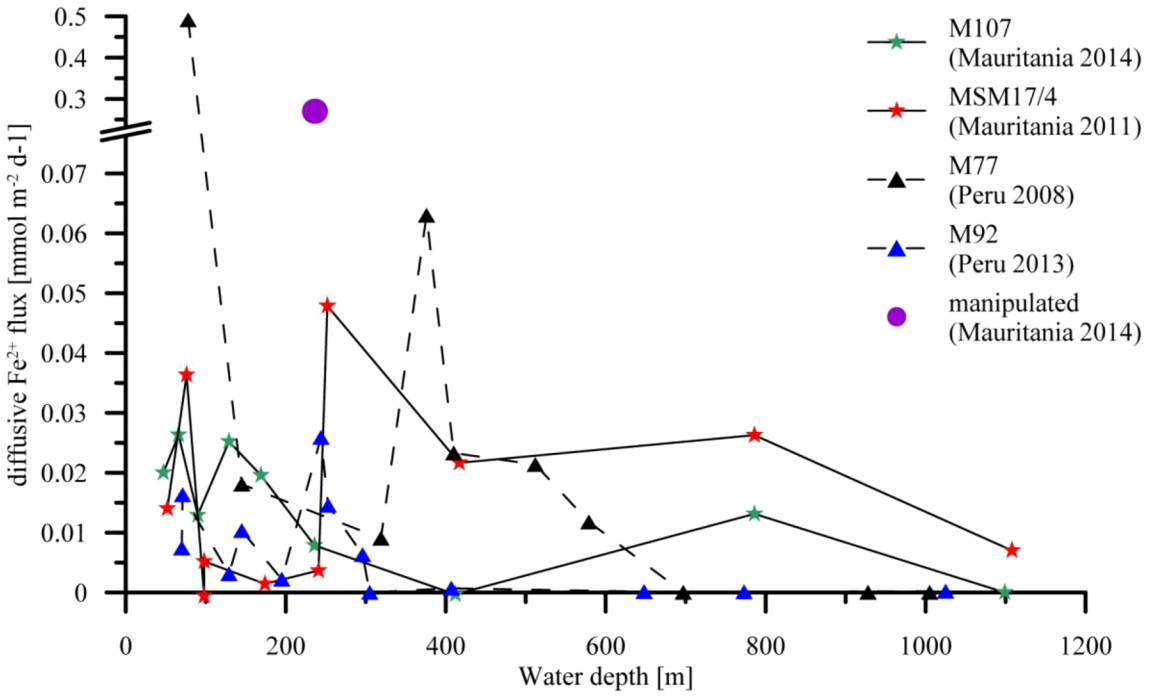

Figure 10: Diffusive Fe^{2+} fluxes (mmol m^{-2} d^{-1}) from Mauritania (MSM17/4 and M107) along the 18°N depth transect and from the Peruvian margin (M77 and M92). The single purple circle denotes the Fe release determined from the O_2 manipulation experiments.

6. 3 Ex situ deoxygenation experiments

In order to estimate the TPO_4^{3-} and Fe^{2+} release potential of the Mauritanian sediments under anoxic conditions, we conducted ex situ deoxygenation experiments. The TPO_4^{3-} release into the bottom water reached 0.15 ± 0.04 mmol m^{-2} d^{-1} after less than 9 days without oxygen, which is less intense than the fluxes found off Peru, but still a significant release rate (Fig. 9 and Tab. 5, Noffke et al., 2012; Lomnitz et al., 2016). The Fe^{2+} release was unverifiable (Fe^{2+} concentrations remained below the detection limit of 100 nM) in the presence of dissolved oxygen. This experimental observation confirms that ferrous iron diffusing from the sediment is rapidly oxidized at the sediment/water interface before it can enter oxygen-bearing bottom waters. Hence, the diffusive Fe^{2+} fluxes calculated from pore water gradients may not represent actual fluxes and may overestimate the iron release from sediments. However, the Fe^{2+} release increased dramatically to 0.27 mmol m^{-2} d^{-1} after O_2, NO_3^-, and NO_2^- were consumed, which falls in the same order of magnitude as the maximum flux measured off Peru (Fig. 10, Tab. 5). This result implies a significant release potential of dissolved TPO_4^{3-} and Fe^{2+} from the sediments on the Mauritanian margin upon deoxygenation and nitrate loss and underlines the need for future studies on benthic nutrient release with respect to changing environmental conditions and their role in ocean deoxygenation.

Conclusions

Benthic TPO_4^{3-} and Fe^{2+} release within the Mauritanian upwelling system is largely controlled by the rate of organic matter degradation in the surface sediment. In addition, sediment characteristics seem to have a certain impact on benthic fluxes while the effect of bottom water oxygenation is low. We suspect that, specifically on the shelf, fluxes across the sediment bottom water interface were enhanced by intense bioirrigation as well as bottom water percolation through permeable surface sediments induced by bottom currents and topography. P mass balance calculations reveal a P deficit at 240 m water depth that could be a result of intense downslope transport of P containing particles contributing to the P burial flux at this station or a lower TPP/POC ratio of the sinking particles compared to the suspended particles that we analyzed. Moreover, comparing TPO_4^{3-} and Fe^{2+} fluxes from 2011 and 2014 revealed only slight differences that are likely induced by higher bottom water oxygen concentrations during the first sampling campaign. Ex situ deoxygenation experiments resulted in P and Fe fluxes comparable in magnitude to naturally occurring benthic fluxes in the OMZ offshore Peru where the water column is fully anoxic most of the time. The results presented here indicate the potential for enhanced nutrient release from sediments underneath the Mauritanian OMZ during progressive deoxygenation of overlying waters. This information could be included in regional models to investigate how the productivity of the overall upwelling system will be affected by changing sediment nutrient release on longer time scales.

Acknowledgements

We are very grateful to the crew of RV *Meteor* during cruise M107 and the crew of RV *Maria S. Merian* during cruise MSM17/4 for the support. Our thanks also go to A. Petersen, M. Türk, and S. Cherednichenko for their assistance in deploying the landers. For their enthusiastic help and cooperation during biogeochemical analyses on board and in the home laboratory, we thank B. Domeyer, V. Thönissen, S. Trinkler, S. Kriwanek, A. Bleyer, R. Suhrberg. This work is a contribution to the Sonderforschungsbereich 754 "Climate – Biogeochemistry Interactions in the Tropical Ocean" (www.sfb754.de), which is supported by the Deutsche Forschungsgemeinschaft.

Author's contributions

U. Lomnitz, A. W. Dale, S. Sommer and D. Clemens conducted the shipboard work and geochemical analysis, and contributed to the manuscript. C. Hensen, K. Wallmann, F. Scholz and A. Noffke contributed to the interpretation and discussion of the data and helped with the manuscript preparation.

References

Aspila, K. I., H. Agemian and A. S. Y. Chau (1976), A semi-automated Method for the Determination of Inorganic, Organic and Total Phosphate in Sediments, Analyst, 101, 187-197, https://doi.org/10.1039/AN9760100187.

Baker, A. R., T. D. Jickells, M. Witt and K. L. Linge (2006), Trends in the solubility of iron, aluminium, manganese and phosphorus in aerosol collected over the Atlantic Ocean, Marine Chemistry, 98(1), 43-58, https://doi.org/10.1016/j.marchem.2005.06.004.

Barton, E. D., J. Arístegui, P. Tett, M. Cantón, J. García-Braun, S. Hernández-León, L. Nykjaer, C. Almeida, J. Almunia, S. Ballesteros, G. Basterretxea, J. Escánez, L. García-Weill, A. Hernández-Guerra, F. López-Laatzen, R. Molina, M. F. Montero, E. Navarro-Pérez, J. M. Rodríguez, K. van Lenning, H. Vélez and K. Wild (1998), The transition zone of the Canary Current upwelling region, Progress in Oceanography, 41, 455-504, https://doi.org/10.1016/S0079-6611(98)00023-8.

Behrenfeld, M. J. and P. G. Falkowski (1997), Photosynthetic rates derived from satellite-based chlorophyll concentration, Limnology and Oceanography, 42(1), 1-20, http://dx.doi.org/10.4319/lo.1997.42.1.0001.

Bell, R. J., R. T. Short and R. H. Byrne (2011), In situ determination of total dissolved inorganic carbon by underwater membrane introduction mass spectrometry, Limnology and Oceanography Methods, 9, 164–175, http://dx.doi.org/10.4319/lom.2011.9.164.

Berelson, W., J. McManus, K. Coale, K. Johnson, D. Burdige, T. Kilgore, D. Colodner, F. Chavez, R. Kudela and J. Boucher (2003), A time series of benthic flux measurements from Monterey Bay, CA, Continental Shelf Research, 23(5), 457-481, https://doi.org/10.1016/S0278-4343(03)00009-8.

Berghuis, E. M., G. C. A. Duineveld and J. Hegeman (1993), Primary production and distribution of phytopigments in the water column and sediments on the upwelling shelf off the Mauritanian coast (Northwest Africa), Hydrobiologia, 258(1), 81-93, doi: 10.1007/bf00006188.

Boyle, E.A. (1983), Chemical accumulation variations under the Peru Current during the past 130,000 years, J. Geophysical Research, 88, C12, 7667-7680, doi: 10.1029/JC088iC12p07667.

Brock, J. and H. N. Schulz-Vogt (2011), Sulfide induces phosphate release from polyphosphate in cultures of a marine Beggiatoa strain, The Isme Journal 5, 497, doi:10.1038/ismej.2010.135.

Broecker, W. S. (1982), Glacial to interglacial changes in ocean chemistry, Progress in Oceanography, 11(2), 151-197, https://doi.org/10.1016/0079-6611(82)90007-6.

Canfield, D. E. (1989), Reactive iron in marine sediments. *Geochimica et Cosmochimica Acta* 53, 619-632, https://doi.org/10.1016/0016-7037(89)90005-7.

Carr, M.-E. (2001), Estimation of potential productivity in Eastern Boundary Currents using remote sensing, Deep Sea Research Part II: Topical Studies in Oceanography, 49(1–3), 59-80, https://doi.org/10.1016/S0967-0645(01)00094-7.

Cropper, T. E., E. Hanna and G. R. Bigg (2014), Spatial and temporal seasonal trends in coastal upwelling off Northwest Africa, 1981–2012, Deep Sea Research Part I: Oceanographic Research Papers, 86, 94-111, https://doi.org/10.1016/j.dsr.2014.01.007.

Dale, A. W., V. J. Bertics, T. Treude, S. Sommer and K. Wallmann (2013), Modeling benthic–pelagic nutrient exchange processes and porewater distributions in a seasonally hypoxic sediment: evidence for massive phosphate release by Beggiatoa?, Biogeosciences, 10(2), 629-651, https://doi.org/10.5194/bg-10-629-2013.

Dale, A. W., S. Sommer, E. Ryabenko, A. Noffke, L. Bohlen, K. Wallmann, K. Stolpovsky, J. Greinert and O. Pfannkuche (2014), Benthic nitrogen fluxes and fractionation of nitrate in the Mauritanian oxygen minimum zone (Eastern Tropical North Atlantic), Geochimica et Cosmochimica Acta, 134(0), 234-256, https://doi.org/10.1016/j.gca.2014.02.026.

Dale, A. W., S. Sommer, U. Lomnitz, I. Montes, T. Treude, V. Liebetrau, J. Gier, C. Hensen, M. Dengler, K. Stolpovsky, L. D. Bryant and K. Wallmann (2015), Organic carbon production, mineralisation and preservation on the Peruvian margin, Biogeosciences, 12(5), 1537-1559, https://doi.org/10.1016/j.gca.2014.02.026.

Emerson, D. (2015), The Irony of Iron – Biogenic Iron Oxides as an Iron Source to the Ocean,
Frontiers in Microbiology, 6, 1502, doi: 10.3389/fmicb.2015.01502.

Elrod, V. A., W. M. Berelson, K. H. Coale and K. S. Johnson (2004), The flux of iron from continental shelf sediments: A missing source for global budgets, Geophysical Research Letters, 31(12), doi:10.1029/2004GL020216.

Faul, K. L., A. Paytan and M. L. Delaney (2005), Phosphorus distribution in sinking oceanic particulate matter, Marine Chemistry, 97(3–4), 307-333, https://doi.org/10.1016/j.marchem.2005.04.002.

Fischer, G., C. Reuter, G. Karakas, N. Nowald and G. Wefer (2009), Offshore advection of particles within the Cape Blanc filament, Mauritania: Results from observational and modelling studies, Progress in Oceanography, 83(1–4), 322-330, https://doi.org/10.1016/j.pocean.2009.07.023.

Förster, A.: Geotechnical measurements to characterise slope sediments and to identify landslide mechanisms and their impact on ecosystems, PhD dissertation, Bremen University, Bremen, 2011.

Froelich, P.N., G.P. Klinkhammer, M.L. Bender, N.A. Luedtke, G.R. Heath, D. Cullen, P. Dauphin, D. Hammond, B. Hartman and V. Maynard (1979), Early oxidation of organic matter in pelagic sediments of the eastern equatorial Atlantic: suboxic diagenesis. Geochimica et Cosmochimica Acta 43, 1075-1090, doi: 10.1016/0016-7037(79)90095-4.

Gier, J., C. R. Löscher, A. W. Dale, S. Sommer, U. Lomnitz, and T. Treude (2017), Benthic Dinitrogen Fixation Traversing the Oxygen Minimum Zone off Mauritania (NW Africa). Frontiers in Marine Science 4 (390), https://doi.org/10.3389/fmars.2017.00390.

Glud, R. N. (2008), Oxygen dynamics of marine sediments, Marine Biology Research, 4(4), 243-289, https://doi.org/10.1080/17451000801888726.

Graco, M., S. Purca, B. Dewitte, C.G. Castro, O. Morón, J. Ledesma, G. Flores, and D. Gutiérrez (2017), The OMZ and nutrients features as a signature of interannual and low-frequency variability off the Peruvian upwelling system, Biogeosciences, 14, 4601-4617, https://doi.org/10.5194/bg-14-4601-2017.

Gutiérrez, D., E. Enríquez, S. Purca, L. Quipúzcoa, R. Marquina, G. Flores, and M. Graco (2008), Oxygenation episodes on the continental shelf of central Peru: Remote forcing and benthic ecosystem response, Progress in Oceanography, 79(2–4), 177-189, https://doi.org/10.1016/j.pocean.2008.10.025.

Hartmann, M., P. J. Müller, E. Suess, and C. H. van der Weijden (1976), Chemistry of Late Quaternary sediments and their interstitial waters of sediment cores from the North-West African continental margin, in Supplement to: Hartmann, M et al. (1976): Chemistry of Late Quaternary sediments and their interstitial waters from the northwest African continental margin. Meteor Forschungsergebnisse, Deutsche Forschungsgemeinschaft, Reihe C Geologie und Geophysik, Gebrüder Bornträger, Berlin, Stuttgart, C24, 1-67, edited, PANGAEA.

Helly, J. J., and L. A. Levin (2004), Global distribution of naturally occurring marine hypoxia on continental margins, Deep Sea Research Part I: Oceanographic Research Papers, 51(9), 1159-1168, https://doi.org/10.1016/j.dsr.2004.03.009.

Ingall, E., and R. Jahnke (1994), Evidence for enhanced phosphorus regeneration from marine sediments overlain by oxygen depleted waters, Geochimica et Cosmochimica Acta, 58(11), 2571-2575, https://doi.org/10.1016/0016-7037(94)90033-7.

Ingall, E., and R. Jahnke (1997), Influence of water-column anoxia on the elemental fractionation of carbon and phosphorus during sediment diagenesis, Marine Geology, 139(1–4), 219-229, https://doi.org/10.1016/S0025-3227(96)00112-0.

Klar, J. K., W. B. Homoky, P. J. Statham, A. J. Birchill, E. L. Harris, E. M. S. Woodward, B. Silburn, M. J. Cooper, R. H. James, D. P. Connelly, F. Chever, A. Lichtschlag and C. Graves (2017), Stability of dissolved and soluble Fe(II) in shelf sediment pore waters and release to an oxic water column, Biogeochemistry, 1-19, doi: 10.1007/s10533-017-0309-x.

Kristensen, E., G. Penha-Lopes, M. Delefosse, T. Valdemarsen, C. O. Quintana and G. T. Banta (2012), What is bioturbation? The need for a precise definition for fauna in aquatic sciences, Marine Ecology Progress Series, 446, 285-302, https://doi.org/10.3354/meps09506.

Li, Y.-H., and S. Gregory (1974), Diffusion of ions in sea water and in deep-sea sediments, Geochimica et Cosmochimica Acta, 38(5), 703-714, https://doi.org/10.1016/0016-7037(74)90145-8.

Lomnitz, U., S. Sommer, A. W. Dale, C. R. Löscher, A. Noffke, K. Wallmann and C. Hensen (2016), Benthic phosphorus cycling in the Peruvian oxygen minimum zone, Biogeosciences, 13(5), 1367-1386, https://doi.org/10.5194/bg-13-1367-2016.

Martin, J. H. (1990), Glacial-interglacial CO2 change: The Iron Hypothesis, Paleoceanography, 5(1), 1-13, doi: 10.1029/PA005i001p00001.

McLennan, S. M. (2001), Relationships between the trace element composition of sedimentary rocks and upper continental crust, Geochemistry, Geophysics, Geosystems, 2(4), doi: 10.1029/2000GC000109.

McManus, J., W. M. Berelson, K. H. Coale, K. S. Johnson and T. E. Kilgore (1997), Phosphorus regeneration in continental margin sediments, Geochimica et Cosmochimica Acta, 61(14), 2891-2907, https://doi.org/10.1016/S0016-7037(97)00138-5.

Mittelstaedt, E. (1983), The upwelling area off Northwest Africa—A description of phenomena related to coastal upwelling, Progress in Oceanography, 12(3), 307-331, doi: https://doi.org/10.1016/0079-6611(83)90012-5.

Moore, W.S., 1987. 228Ra in the South-Atlantic Bight. Journal of Geophysical Research-Oceans, 92(C5): 5177-5190, https://doi.org/10.1029/JC092iC05p05177.

Moore, W.S. and Arnold, R., 1996b. Measurement of 223Ra and 224Ra in coastal waters using a delayed coincidence counter. Journal of Geophysical Research-Oceans, 101(C1): 1321-1329, https://doi.org/10.1029/95JC03139.Morel, A., D. Antoine, M. Babin and Y. Dandonneau (1996), Measured and modeled primary production in the northeast Atlantic (EUMELI JGOFS program): the impact of natural variations in photosynthetic parameters on model predictive skill, Deep Sea Research Part I: Oceanographic Research Papers, 43(8), 1273-1304, https://doi.org/10.1016/0967-0637(96)00059-3.

Noffke A., C. Hensen, S. Sommer, F. Scholz, L. Bohlen, T. Mosch, M. Graco and K. Wallmann (2012), Benthic iron and phosphorus fluxes across the Peruvian oxygen minimum zone, Limnology and Oceanography, 57(3), 851-867, doi: 10.4319/lo.2012.57.3.0851.

Norkko, J. and Shumway, S. E. (2011). Bivalves as bioturbators and bioirrigatiors, In: Sandra E. Shumway (Ed.), Shellfish Aquaculture and the Environment, First Edition, pp.297-312. John Wiley & Sons, Inc. doi:10.1002/9780470960967

Ohnemus, D. C. and P. J. Lam (2015), Cycling of lithogenic marine particles in the US GEOTRACES North Atlantic transect, Deep Sea Research Part II: Topical Studies in Oceanography, 116, 283-302, https://doi.org/10.1016/j.dsr2.2014.11.019.

Oschlies, A., K. G. Schulz, U. Riebesell and A. Schmittner (2008), Simulated 21st century's increase in oceanic suboxia by CO2-enhanced biotic carbon export, Global Biogeochemical Cycles, 22(4), GB4008, doi: 10.1029/2007GB003147.

Pauly, D. and V. Christensen (1995), Primary production required to sustain global fisheries, Nature, 374(6519), 255-257, doi: 10.1038/374255a0.

Paytan, A. and K. McLaughlin (2007), The Oceanic Phosphorus Cycle, Chemical Reviews, 107(2), 563-576, doi: 10.1021/cr0503613.

Rama and Moore, W.S., 1996. Using the radium quartet for evaluating groundwater input and water exchange in salt marshes. Geochimica Et Cosmochimica Acta, 60(23): 4645-4652, https://doi.org/10.1016/S0016-7037(96)00289-X.

Redfield, A. C., B. H. Ketchum and F. A. Richards (1963), The influence of organisms on the composition of seawater, in The Sea, edited by N. M. Hill, pp. 26-77, Academic Press, London.

Ruttenberg, K. C. and R. A. Berner (1993), Authigenic apatite formation and burial in sediments from non-upwelling, continental margin environments, Geochimica et Cosmochimica Acta, 57(5), 991-1007, https://doi.org/10.1016/0016-7037(93)90035-U.

Scheuvens, D., L. Schütz, K. Kandler, M. Ebert and S. Weinbruch (2013), Bulk composition of northern African dust and its source sediments — A compilation, Earth-Science Reviews, 116, 170-194, https://doi.org/10.1016/j.earscirev.2012.08.005.

Schmidtko, S., L. Stramma and M. Visbeck (2017), Decline in global oceanic oxygen content during the past five decades, Nature, 542(7641), 335-339, doi:10.1038/nature21399.

Scholz, F., J. McManus, A. C. Mix, C. Hensen and R. R. Schneider (2014), The impact of ocean deoxygenation on iron release from continental margin sediments, Nature Geosci, 7(6), 433-437, doi:10.1038/ngeo2162.

Scholz, F., C. Hensen, A. Noffke, A. Rohde, V. Liebetrau and K. Wallmann (2011), Early diagenesis of redox-sensitive trace metals in the Peru upwelling area – response to ENSO-related oxygen fluctuations in the water column, Geochimica et Cosmochimica Acta, 75(22), 7257-7276, https://doi.org/10.1016/j.gca.2011.08.007.

Scholz, F., Löscher, C. R., A. Fiskal, S. Sommer, C. Hensen, U. Lomnitz, K. Wuttig, J. Göttlicher, E. Kossel, R. Steininger and D. E. Canfield (2016), Nitrate-dependent iron oxidation limits iron transport in anoxic ocean regions, Earth and Planetary Science Letters, 454, 272-281, https://doi.org/10.1016/j.epsl.2016.09.025.

Schulz, H. N., and H. D. Schulz (2005), Large Sulfur Bacteria and the Formation of Phosphorite, Science, 307(5708), 416-418, doi: I10.1126/science.1103096.

Schunck, H., G. Lavik, D. Dhwani K., T. Großkopf, T. Kalvelage, C. R. Löscher, A. Paulmier, S. Contreras, H. Siegel, M. Holtappels, P. Rosenstiel, M. B. Schilhabel, M. Graco, R. A. Schmitz, M. M. M. Kuypers and J. LaRoche (2013), Giant Hydrogen Sulfide Plume in the Oxygen Minimum Zone off Peru Supports Chemolithoautotrophy, PLOS ONE, 8(8), doi: 10.1371/journal.pone.0068661.

Severmann, S., J. McManus, W. M. Berelson and D. E. Hammond (2010), The continental shelf benthic iron flux and its isotope composition, Geochimica et Cosmochimica Acta, 74(14), 3984-4004, https://doi.org/10.1016/j.gca.2010.04.022.

Slomp, C. P., Malschaert, J. F. P. and Van Raaphorst, W. (1998), The role of adsorption in sediment-water exchange of phosphate in North Sea continental margin sediments, Limnology and Oceanography, 43, 832–846, doi: 10.4319/lo.1998.43.5.0832.

Sokoll, S., G. Lavik, S. Sommer, T. Goldhammer, M. M. M. Kuypers and M. Holtappels (2016), Extensive nitrogen loss from permeable sediments off North-West Africa, Journal of Geophysical Research: Biogeosciences, 121(4), 1144-1157, doi: 10.1002/2015JG003298.

Sommer, S., P. Linke, O. Pfannkuche, T. Schleicher, S. v. Deimling, A. Reitz, M. Haeckel, S. Flögel and C. Hensen (2009), Seabed methane emissions and the habitat of frenulate tubeworms on the Captain Arutyunov mud volcano (Gulf of Cadiz), Marine Ecology Progress Series, 382, 69-86, https://doi.org/10.3354/meps07956.

Sommer S., J. Gier, T. Treude, U. Lomnitz, M. Dengler, J. Cardich and A. W. Dale (2016), Depletion of oxygen, nitrate and nitrite in the Peruvian oxygen minimum zone cause an imbalance of benthic nitrogen fluxes, Deep-Sea Research 112, 113-122 https://doi.org/10.1016/j.dsr.2016.03.001.

Sommer S., D. Clemens, M. Yücel, O. Pfannkuche, P. O. J. Hall, E. Almroth-Rosell, H. N. Schulz-Vogt and A. W. Dale (2017), Major Bottom Water Ventilation Events Do Not Significantly Reduce Basin-Wide Benthic N and P Release in the Eastern Gotland Basin (Baltic Sea), Frontiers in Marine Science, 4, 18, doi: 10.3389/fmars.2017.00018.

Stookey, L. L. (1970), Ferrozine---a new spectrophotometric reagent for iron, Analytical Chemistry, 42(7), 779-781, doi: 10.1021/ac60289a016.

Stramma, L., G. C. Johnson, J. Sprintall and V. Mohrholz (2008), Expanding Oxygen-Minimum Zones in the Tropical Oceans, Science, 320(5876), 655-658, doi: 10.1126/science.1153847.

Sundby, B., L. G. Anderson, P. O. J. Hall, Å. Iverfeldt, M. M. R. van der Loeff and S. F. G. Westerlund (1986), The effect of oxygen on release and uptake of cobalt, manganese, iron and phosphate at the sediment-water interface, Geochimica et Cosmochimica Acta, 50(6), 1281-1288, https://doi.org/10.1016/0016-7037(86)90411-4.

Wallmann, K. (2010), Phosphorus imbalance in the global ocean?, Global Biogeochemical Cycles, 24(4), doi: 10.1029/2009GB003643.

Zabel, M., T. Bickert, L. Dittert and R. R. Haese (1999). Significance of the sedimentary Al:Ti ratio as an indicator for variations in the circulation patterns of the equatorial North Atlantic. Paleoceanography 14, 789-799, doi:10.1029/1999PA900027.

Tables

Table 1 Station list including geographical coordinates, sampling date, water depths and bottom water oxygen concentration for all sites along the 18°N depth transect from cruises M107 (June 2014) and MSM17/4 (March – April 2011).

No.	Station	Gear	Lat. N	Long. W	Date	Water depth (m)	Bottom water O_2 (µM)
Cruise M107							
1	658	MUC13	18°17.299'	16°18.994'	23.06.14	47	50
	665	BIGO2-4	18°17.100'	16°18.997'	23.06.14	47	
2	686	MUC19	18°16.287'	16°22.910	25.06.14	66	27
	688	BIGO2-5	18°16.286	16°22.932'	25.06.14	67	
3	628	MUC10	18°15.197'	16°27.002'	21.06.14	90	25
	630	BIGO1-3	18°15.006'	16°27.010'	21.06.14	91	
4	672	MUC17	18°14.483'	16°29.634'	24.06.14	129	35
	673	BIGO1-4	18°14.485'	16°29.635'	24.06.14	129	
5	697	MUC20	18°14.299'	16°30.995'	26.06.14	169	42
	617	BIGO2-3	18°14.397'	16°31.000'	20.06.14	171	
6	612	MUC8	18°12.945'	16°33.153'	20.06.14	236	53
	598	BIGO1-2	18°13.286'	16°33.334'	15.06.14	236	
	583	MUC7A	18°12.998'	16°33.197'	14.06.14	237	50
	583	MUC7B	18°12.998'	16°33.197'	14.06.14	237	
	583	MUC7C	18°12.998'	16°33.197'	14.06.14	237	
7	554	MUC5	18°12.504'	16°35.583'	12.06.14	412	46
	557	BIGO2-2	18°12.504'	16°35.585'	12.06.14	412	
8	534	MUC3	18°11.288'	16°39.328'	10.06.14	786	72
	547	BIGO1-1	18°11.31'	16°39.335'	11.06.14	787	
9	527	BIGO2-1	18°10'	16°44.99'	09.06.14	1096	132
	669	MUC15	18°10.001'	16°44.997'	24.06.14	1099	
	524	MUC1	18°09.991'	16°45.023'	09.06.14	1108	
Cruise MSM17/4							
	485	BIGO 1-4	18°17.30'	16°19.01'	28.03.11	53	56
	463	MUC35	18°17.30'	16°19.01'	25.03.11	52	
	409	BIGO1-2	18°15.20'	16°27.00'	20.03.11	98	59
	406	MUC25	18°15.23'	16°27.00'	20.03.11	98	
	560	MUC52	18°14.31'	16°27.03'	17.04.11	98	
	539	BIGO2-4	18°14.30'	16°31.01'	04.04.11	174	57
	536	MUC50	18°14.30'	16°31.01'	04.04.11	174	
	466	BIGO2-1	18°13.10'	16°33.30'	21.03.11	241	57
	421	MUC28	18°13.05'	16°33.30'	21.03.11	241	
	584	MUC53	18°12.90'	16°33.30'	08.04.11	255	
	453	BIGO1-3	18°12.54'	16°35.65'	24.03.11	425	53
	448	MUC31	18°12.56'	16°35.60'	24.04.11	417	

530	BIGO1-5	18°11.29'	16°39.32'	03.04.11	789	
506	MUC44	18°11.31'	16°39.32'	31.03.11	786	
466	BIGO2-2	18°10.00'	16°45.00'	25.03.11	1113	139
483	MUC36	18°10.00'	16°45.00'	28.03.11	1108	

Table 2 Average sedimentary Fe/Al and Ti/Al ratios in sediment cores from each station along the depth transect.

Station	Water depth (m)	Fe/Al	Ti/Al
659 MUC 14	47	0.47	0.068
686 MUC 19	66	0.51	0.073
628 MUC 10	90	0.63	0.077
672 MUC 17	129	0.62	0.071
697 MUC 20	169	0.61	0.074
583 MUC 7C	236	0.57	0.074
554 MUC 5	412	0.5	0.06
534 MUC 3	786	0.5	0.06
524 MUC 1	1108	0.51	0.06
Average Fe/Al		**0.55**	**0.07**

Table 3 Benthic chamber TPO_4^{3-} and DIC fluxes and diffusive TPO_4^{3-} and Fe^{2+} fluxes from cruise M107 and MSM17/4. The error given for the benthic fluxes is the difference of the fluxes from two benthic chambers in each BIGO lander. Diffusive fluxes were calculated according to Eq. (1) section 4.3. Units are in mmol m^{-2} d^{-1}.

No.	Station	Gear	Benthic chamber TPO_4^{3-} flux	Diffusive TPO_4^{3-} flux	Diffusive Fe^{2+} flux	Benthic chamber DIC flux
Cruise M107						
1	658	MUC13		0.02	0.02	
	665	BIGO2-4	0.2 ± 0.07			20.06 ± 0.69
2	686	MUC19		0.04	0.03	
	688	BIGO2-5	0.17 ± 0.03			15.34 ± 2.67
3	628	MUC10		0.01	0.01	
	630	BIGO1-3	0.09 ± 0.05			10.75 ± 2.15
4	672	MUC17		0.03	0.03	
		BIGO1-4	0.16 ± 0.01			9.52 ± 1.03
5	697	MUC20		0.04	0.02	
	617	BIGO2-3	0.14 ± 0.03			7.93 ± 0.69
6	612	MUC8		0.02	0.01	
	598	BIGO1-2	0.11 ± 0.05			8.64 ± 0.07
7	554	MUC5		0.01	0	
	557	BIGO2-2	0.08 ± 0.02			5.64 ± 2.5
8	534	MUC3		0.03	0.01	
	547	BIGO1-1	0.05 ± 0.01			5.8 ± 1.2
9	527	BIGO2-1	0.06 ± 0.01			5.86 ± 2.3
	669	MUC15		0.02	0	
	524	MUC1		0.02	0	
Cruise MSM17/4						
	463	MUC35			0.01	
	485	BIGO 1-4	0.04			
	406	MUC25			0.01	
	560	MUC52			0	
	425	BIGO1-2	0			
	536	MUC50			0	
	539	BIGO2-4	0.11±0.02			
	421	MUC28			0	
	584	MUC53			0.05	
	466	BIGO2-1	0.055±0.025			
	448	MUC31			0.02	
	453	BIGO1-3	0.11±0.01			
	506	MUC44			0.03	
	530	BIGO1-5	0.06±0.01			
	483	MUC36			0.01	
	466	BIGO2-2	0.07±0			

Table 4 POC/TPP, POC/PIP and POC/POP ratios for water column particles, collected at St. 1 and 5, and surface sediments of all stations along the depth transect. The error given for the water column particle ratios was determined from two filter samples taken in each sampling depth.

Station	Water depth	Sampling depth (m) / water depth) (cm) / sediment depth	POC/TPP	POC/PIP	POC/POP
Water column particles					
645 CTD 46	46	10	98 ±1	160 ± 14	264 ± 44
645 CTD 46	46	20	87 ± 7	138 ± 36	693 ± 546
645 CTD 46	46	BW	103 ± 8	208 ± 38	235 ± 79
582 CTD 24	233	10	139 ± 24	298 ± 27	264 ± 63
582 CTD 24	233	20	201 ± 51	600 ± 140	376 ± 302
582 CTD 24	233	50	167 ± 6	471 ± 30	250 ± 14
582 CTD 24	233	100	135 ± 7	287 ± 2	257 ± 25
582 CTD 24	233	150	140 ± 0	224 ± 7	375 ± 17
582 CTD 24	233	200	132 ± 12	339 ± 30	225 ± 48
582 CTD 24	233	BW	138 ± 7	376 ± 71	222 ± 7
Average water column particles			**134 ± 12**	**310 ± 40**	**309 ± 87**
Sediments					
659 MUC 14	47	0.5	91	117	408
		1.5	106	121	872
		2.5	55	73	227
		3.5	56	60	1009
		5.5	91	112	492
		7.5	85	106	427
		9.5	67	88	291
686 MUC 19	66	0.5	62	82	243
		1.5	54	80	171
		2.5	64	83	285
		3.5	71	92	321
		5.5	72	97	280
		7.5	72	99	269
		9.5	75	97	336
628 MUC 10	90	1	42	55	185
		3	52	66	251
		7	67	90	267
		9	80	88	840
697 MUC 20	169	0.5	73	97	292
		1.5	78	97	413
		3.5	79	111	272
		5.5	77	106	278
		7.5	76	102	293
		8	87	114	364
583 MUC 7C	236	0.5	82	102	416
		1.5	72	105	234
		2.5	83	108	362
		3.5	76	121	205
		5.5	89	127	292
		7.5	89	123	319
		9.5	84	106	416
554 MUC 5	412	0.5	81	115	271
		1.5	77	87	682
		3.5	89	123	322
		5.5	86	121	297
		7.5	95	135	324
		9.5	90	126	317
534 MUC 3	786	0.25	90	119	364
		0.75	82	111	309
		2.25	95	144	278
		3.75	99	154	281
		5.5	108	154	359
		7.5	127	161	603
		8	122	185	357
524 MUC 1	1108	0.25	83	120	271
		0.75	89	127	299
		2.25	96	144	286
		3.75	112	168	338
		5.5	117	181	332
		7.5	127	200	349

Table 5. TPO_4^{3-} and Fe^{2+} fluxes to the in the overlying waters the ex situ O_2 manipulation experiment at St 6.

Core	Incubation time TPO_4^{3-} (h)	Diffusive TPO_4^{3-} flux (mmol m^{-2} d^{-1})	Average TPO_4^{3-} flux (mmol m^{-2} d^{-1})	Incubation time Fe^{2+} (h)	Diffusive Fe^{2+} flux (mmol m^{-2} d^{-1})	Average Fe^{2+} flux (mmol m^{-2} d^{-1})
A	97-255	0.19		133-247	0.35	
			0.15 ± 0.04			**0.27 ± 0.08**
B	113-279	0.11		151-267	0.19	

Table 6 P mass-balance at St. 1 (47 m) and 6 (236 m).

Parameter	Calculation	St. 1	St. 2
Total benthic chamber P release **TPO_4^{3-} flux** (mmol m^{-2} d^{-1})	measured	0.2 ± 0.07	0.11 ± 0.05
P release form POP degradation **TPO_4^{3-} (POP)** (mmol m^{-2} d^{-1})	$TPO_{4\,(POP)}^{3-} = DIC\,/(\frac{POC}{POP})$ $\frac{POC}{POP}$ is the ratio of particles collected in the bottom water (lowest sample in water column)	0.09 ± 0.003	0.04 ± 0
P release form TPP degradation **TPO_4^{3-} (TPP, WC)** (mmol m^{-2} d^{-1})	$TPO_{4\,(TPP,WC)}^{3-} = DIC\,/(\frac{POC}{TPP})$ $\frac{POC}{TPP}$ is the ratio of particles collected in the bottom water (lowest sample in water column)	0.15 ± 0.006	0.08 ± 0.001
Sedimentation rate **SR** (cm yr^{-1})	Dale et al., 2013	0	0.35
Mass accumulation rate **MAR** (g cm^{-2} yr^{-1})	$MAR = \rho\,(1-\phi)SR$ with: ρ = 1.8 (dry bulk density (g cm^{-3}) from Förster, 2011) ϕ = 0.49 (porosity at the lower core end)	0	0.32
P burial **P_{tot}** (mmol m^{-2} d^{-1})	$P_{tot} = MAR * [P_{10}]$ P_{10} = (P concentration in 10 cm depth, Supplement 2)	0	0.08
P release from the dissolution of Fe (oxyhydr)oxides **TPO_4^{3-} (Fe)** (mmol m^{-2} d^{-1})	$TPO_{4\,(Fe)}^{3-} = Fe^{2+}/\left(\frac{Fe}{P}\right)$ ($\frac{Fe}{P}$ = 10, Slomp et al., 1996)	0.0083	0.0037
P from terrigenous input **TPO_4^{3-} (terr)** (mmol m^{-2} d^{-1})	$TPO_{4\,(terr)}^{3-} = MAR * [Al_{0-1}] * \frac{P}{Al}$ $Al_{0\text{-}1}$ = 0.84 mmol g^{-1} (Al concentration of surface sediment, Supplement 1) $\frac{P}{Al}$ = 0.01 (ratio of P and Al in the surface sediment, Supplement 1)	0	7.4 x 10^{-6}
P deficit **TPO_4^{3-} (def)** (mmol m^{-2} d^{-1})	$TPO_{4\,(def)}^{3-} = TPO_{4\,(TPP,WC)}^{3-} + TPO_{4\,(Fe)}^{3-} + TPO_{4\,(terr)}^{3-} - (TPO_4^{3-} + P_{tot})$	0.04	0.1

Highlights:

- next to organic matter degradation, bioirrigation and bottom water percolation through permeable surface sediments enhances benthic TPO_4^{3-} and Fe^{2+} release
- changes in bottom water oxygenation induce slight changes benthic TPO_4^{3-} and Fe^{2+} release rates measured in 2011 and 2014
- deoxygenation experiments imply enhanced TPO_4^{3-} and Fe^{2+} release at ongoing deoxygenation in the Mauritanian OMZ